UNIVERSITÀ DEGLI STUDI DI TORINO

Revisiting the last major eruptions of Stromboli volcano: inferences on the role of volatiles during magma storage and decompression.

In Zellmer, G. F., Edmonds, M. & Straub, S. M. (eds) The Role of Volatiles in the Genesis, Evolution and Eruption of Arc Magmas. Geological Society, London, Special Publications, 410, 143-177, First published online August 6, 2014

By

Cigolini C., Laiolo M., Coppola D. (2014)

http://dx.doi.org/10.1144/SP410.3

Revisiting the last major eruptions at Stromboli volcano: inferences on the role of volatiles during magma storage and decompression

Cigolini C.[1,2], Laiolo M.[1], Coppola D.[1]

1 – Dipartimento di Scienze della Terra, Università di Torino,Via Valperga Caluso 35, 10125 Torino, Italy
2 –NatRisk, Centro Interdipartimentale sui Rischi Naturali in Ambiente Montano e Collinare, Universita` degli Studi di Torino, Italy

Correspondig Author: Corrado Cigolini

Email: corrado.cigolini@unito.it; Phone: +39-011670-5107; Fax: +39-011670-5128

Abstract

Stromboli is a unique open conduit volcano and a natural laboratory to investigate how volatiles migrate and concentrate under dynamic conditions. Fluid phases are involved in magma decompression and pressurization, modulate Strombolian activity and rule magma rise and fragmentation processes. Here, we have revisited the available data on the last two major eruptions at Stromboli volcano and concentrated our analysis on the 2007 eruption. First, we further analysed petrological-geochemical data to assess equilibrium conditions by using standard thermobarometry; then we used a grid of selected reactions which involve solid-melt-fluid equilibria to better constrain the P-T regimes that adequately describe our system. Primitive hydrous basaltic melts, reported in literature, and preserved as melt inclusions in olivine (with 2.3-3.8 wt% of H_2O, and 890-1590 p.p.m. CO_2), are equilibrium with forsteritic olivine and a diopsidic clinopyroxene, at average pressures of 260 (±47) MPa for temperatures approaching 1170 (±17) °C, and calculated $X^{m}_{CO_2}$ (mole fraction of CO_2 within the melt) ranging from 0.60 to 0.76. Ca-rich or ultracalcic melts are regarded as a result of decompression along a steep adiabatic and/or isothermal curve. During this process the magma will crosscut the stability field of diopside and enter the liquidus field. The earlier crystallized diopside is destabilized and will react with the coexisting liquid phase leading to

the formation of ultracalcic melts. Ejected golden pumices (with 2-3 wt% H_2O), are in equilibrium with Ca-pyroxene, forsteritic olivine and anorthitic plagioclase at 150–220 MPa and temperatures of 1120-1150°C. Evolved melt inclusions (substantially degassed) in Fe-richer olivine (ca. Fo_{70}) of the scorias show average equilibration pressures of 78 (± 20) MPa, and temperatures 1138 (± 14) °C.

In summary, the higher *P-T* regimes associated with the origin of primitive melt inclusions are representative of the base of the chamber, where the ferromagnesian phases may crystallise and cumulate. The magma with a bulk composition typical of the pumices is stored the middle and main part of the chamber (likely its axial sector) and these materials are erupted during paroxysmal, and more rarely, major explosions. Finally more evolved melts inclusions found in the olivine of the scorias are indicative of crystallisation within the conduit or its root-zone connected with the upper part of the chamber.

Pure extensional regimes and recent geophysical data suggest the existence of a prolate ellipsoidal magma chamber below Stromboli. To constrain its volume we estimated the magma volumes associated with SO_2 degassing (during the 2007 major eruption) by applying a refined petrological model that allowed us to estimate the magma fluxes in the subvolcanic region (i.e., the magma flux entering the degassing zone). The long term trend of this magma flux follows an overall exponential decay, typical of pressurised magmatic systems, and indicated that magma rise was accompanied and followed by a slow decompression. This trend was shown to be consistent release of elastic strain accumulated either by pressurisation of the rocks surrounding the magma reservoir, or by pressurisation of the magma itself, or both. By analyzing the reservoir elastic response during magma decompression, we found that the current Stromboli magma chamber volume may be adequately constrained within 1-2 km^3.

Introduction

The role of volatiles is crucial in controlling petrogenetic and volcanic processes. Among these the most tangible are, for example, partial melting in the source region of primitive magmas, and the dynamics of fragmentation processes in magma chambers and volcanic conduits. Gaseous phases modulate magma transfer toward the surface and are involved in active degassing when magma batches are momentarily stored in the subvolcanic region before reaching the surface. Recent experimental progresses in igneous petrology and physical volcanology gave us the opportunity to refine solubility models to define degassing trajectories, and to better understand vesiculation processes. However, open conduit volcanoes are natural laboratories to investigate how volatiles migrate and concentrate under dynamic conditions. Fluid phases are involved in pressurising reservoirs, rule magma rise and wall-rock fracturing during dike injection that may lead to effusive-explosive eruptions at active volcanoes. A unique case to study these phenomena is Stromboli volcano located in the Tyrrhenian sea.

Stromboli is a composite stratovolcano with a persistent open-system activity used as a reference case by volcanologists to classify minor to intermediate volcanic eruptions (e.g. Newhall and Self, 1982). The role of fluids in modulating strombolian activity is fundamental since it is involved in the so called “gas puffing” when magma pulses reach the open vents. During these phases, the sudden outburst of gaseous phases induces minor explosions with the projection of scoria bombs, lapilli and ash that characterise the typically mild strombolian activity. In addition, more violent events, also known as “major explosions”, are triggered by portions of undegassed magma that reaches the upper part of the conduit and explosively releases the exsolving gases. However, more energetic paroxysmal explosions are strongly linked to fragmentation processes induced by a “nearly instantaneous” ascent of a fluid-saturated *slug* that migrates through the conduit and explosively expands in its upper part.

Stromboli rejuvenated the scientific interest with the onset of major eruptive cycle on December 28, 2002: lava effusion from summit vents was followed, on December 30, by a composite slump down the northern part of the cone, generating a tsunami that damaged part of the village and propagated to the north-eastern coast of Sicily. A multidisciplinary effort was coordinated by Italian Civil Defence authorities to mitigate volcanic risk and the potential effects of tsunami waves in the west-central Mediterranean region. This approach gave the scientific community the opportunity to carefully monitor the last effusive cycle (from February 27 to April 2, 2007) that culminated in the paroxysmal explosion of March 15, 2007.

In this review paper we integrate geophysical and petrological data to refine current models on the inner plumbing system of Stromboli volcano in the attempt to better decode the role of volatiles during magma storage and ascent. We will focus our analyses on available experimental petrologic data, melt inclusions and minerochemical data. We thermodynamically calculated mineral-melt-fluid equilibria on selected reactions to refine thermobarometry and magma compressibility during decompression. This will allow us, by means of geophysical models retrieved by analysing SO_2 emissions, to constrain magma chamber volumes for better interpreting the eruption dynamics.

Fig. 1

Geological Setting

Stromboli is the north-eastern island of the Aeolian Arc and has been built on a rather thin continental crust of the Calabrian arc (Fig. 1). This crustal unit extends westward beneath Lipari and Vulcano and then vanishes below Marsili submarine volcano. Fragments of this crust (quarzite, tonalite and diorite) were found as xenoliths in the older lavas of Stromboli (cf., Laiolo & Cigolini 2006; and references therein). The volcano is located onto the Stromboli-Panarea alignment: a NE-SW fault subsidiary of the Tindari-Letojanni fault that propagates NNW-SSE though Eastern Sicily below Etna volcano (Ventura *et al.*, 1999; De Astis *et al.*, 2003; Acocella *et al.*, 2009). The Aeolian

Islands were built within the last 1.3 my (Gillot & Keller 1993). Lavas and tephra are essentially subduction-related calcalkaline, HK-calcalkaline, shoshonitic and potassic rocks. Subduction of the Ionian plate beneath the Calabrian Arc and was accompanied by a regional uplift (0.5-0.7 my), associated with crustal extension. Uplift within the forearc region was related to the rebound of the upper plate (Calabrian Arc and part of the Ionian lithosphere; e.g., Gvirtzman & Nur 2001). Current subduction is responsible of regional seismicity and volcanism (Fig. 1). A recent systematic analysis of teleseismic data by Pontevivo & Panza (2006) support the idea that the Moho below Stromboli is shallow, and located at about 15-17 km depth. These authors identified a low velocity layer (v_s ~ 3.5 km*sec^{-1}) at a depth of 15-32 km below the cone. However, the source region of Stromboli primitive melts is well deeper, since primitive magmas likely originate in the mantle wedge above the Benioff Zone (e.g. Peccerillo, 2001; Schiavi *et al.*, 2012). Earthquake's subduction-related hypocenters reach a depth of approximately 500 km and cluster at about 350-150 km below Stromboli (Fig. 1, see the INGV data bank ISIDe: Italian Seismological Instrumental and Parametric Data Base at http://iside.rm.ingv.it/iside/standard/result.jsp?rst=1&page=EVENTS). Recently, D'Auria *et al.* (2006) have located, by means of broadband network operative at Stromboli, few seismic events at depths 4.5-6 km below the summit of the volcano. These hypocenters are positioned in the surroundings of the top of the magma reservoir.

Stromboli volcano

The cone of Stromboli is approximately 3 km high with the top reaching 924 m a.s.l. (above sea level). The typical Strombolian activity is characterised by the persistent moderate explosions with the ejection of scoriae, lapilli, ash and bombs from vents positioned at the summit of Sciara del Fuoco (a collapsed sector delimited by a horseshoe-shaped scarp opening north-westward, e.g. Tibaldi *et al.*, 2009). The "mild" and persistent strombolian activity may be interrupted lava effusions, major explosions and paroxysms (Barberi *et al.*, 1993; Bertagnini *et al.*, 2011). A detailed study on the thermal regimes occurring at Stromboli, correlated with changes in volcanic activity

for over a decade, has been reported by Coppola *et al.* (2012). The material erupted during major and paroxysmal explosions consists of high vesicular lapilli and bombs, that are formed by the mingling of dark-coloured and crystal-rich scoria with golden-coloured crystal-poor *pumice* within a subvolcanic chamber (e.g., Francalanci *et al.*, 1999; Métrich *et al.*, 2001; 2005). The pumice contains olivine crystals that bear melt inclusions, likely representing the primitive shoshonitic Stromboli basalts. The April 5, 2003 and March 15, 2007 paroxysmal explosions occurred during both the last two effusive cycles. These explosions have been interpreted as a result of decompression induced by rapid magma discharge that triggered the ascent of a gas-rich deep-seated magma, leading to fragmentation of the pumiceous foam within the open conduit (Ripepe *et al.*, 2005). According to Cigolini *et al.* (2008) this process follows the elastic rebound of the chamber walls that will squeeze up portions of the undegassed magma column (that, in turn, would instantaneously rise and cross-cut the depth where critical gas saturation occurs), leading to magma fragmentation with the ejection of the "primitive golden pumices". The amount of lava discharged during both effusive cycles may be estimated to be around 1-1.3 x 10^7 m^3 (Calvari *et al.*, 2005) and 0.7-1 x 10^7 m^3 (Neri & Lanzafame, 2009; Marsella *et al.*, 2009; Calvari *et al.*, 2010) (Fig. 2). Flank slumping onto Sciara del Fuoco occurred during several recent lava effusions (namely in 1879, 1916, 1919, 1930, 1944 and 1954, according to Barberi *et al.*, 1993) and generated tsunamis waves in this sector of the Mediterranean.

Fig. 2

The cone of Stromboli is subdivided into five units (Hornig-Kjarsgaard *et al.* 1993; Keller *et al.*, 1993; Francalanci *et al.*, 1993) of calc-alkaline type and shoshonitic affinity: three of them refer to the older part of the volcano, known as *Paleostromboli* (110-35 ky). The *Scari* lavas and tephra (34 ± 3 ky in age) are basalts and shoshonite that overlay the Paleostromboli. The *Vancori* lavas

(shoshonitic basalts and trachytes, with ages 26 to 13 ky) lay on top of the above sequence. The *Neostromboli* unit (13-6 ka) is in the northern sector of the island (Fig. 1b) and consists of shoshonitic and potassic lavas. Recent *San Bartolo lavas*, erupted during roman times (Arrighi *et al.*, 2004; Speranza *et al.*, 2008), are high-K calc-alkaline basalts with abundant mafic and ultramafic mantle xenoliths, ascribed to the roots-zone of Stromboli plumbing system (Laiolo & Cigolini 2006). Current lavas and tephra are high-K calc-alkaline basalts and shoshonites (cf., Francalanci *et al.*, 2004; Landi *et al.*, 2009; Pompilio *et al.*, 2012).

Structurally, the architecture of the island is the result of summit collapses of caldera type that took place from 100 to 13 ky BP (e.g., Tibaldi *et al.*, 2009). The last one led to the formation of Sciara del Fuoco (Fig. 1b). Recently, Marsella *et al.* (2012) reconstructed the morphological evolution of the Sciara del Fuoco since 1868, and correlated it with the on-going volcanic activity. Summit vents were persistently (and are currently) located along a N40°E normal fault. This trend is also consistent with the main direction of dyking (e.g., Tibaldi *et al.*, 2003; Ripepe *et al.*, 2005)

The structure of the subvolcanic plumbing system has been recently discussed. According to several authors (Métrich *et al.*, 2001, 2005; 2010), Bertagnini *et al.* (2003), Francalanci *et al.* (2004) the plumbing system is represented by a lower main chamber (that contains the primitive undegassed low porphyritic magma, LP magma, normally ejected as golden pumices) connected to an upper subsidiary reservoir where the more evolved magma is momentarily stored (degassed high porphyritic magma, HP magma, erupted as lavas and/or scorias during effusive and mild strombolian activity). According to Cigolini *et al.* (2008) the geometry of the plumbing system is strongly controlled by the local structural setting and stress distribution, and is simply represented by a prolate ellipsoid connected, in the subvolcanic region, with the active conduit. In this view the primitive LP magma is confined within its lower part, whereas the HP magma is located in its upper portion. However, geophysical data support the occurrence of an ellipsoidal structure below Stromboli volcano (Bonaccorso *et al.*, 2008).

186

187 **Analytical methods**

188 *Mineral phases* and *glasses* of samples collected at Stromboli during 2006 and 2007 were analyzed
189 at the Dipartimento di Scienze della Terra of the University of Torino with a SEM Cambridge
190 Instruments Stereoscan 360 equipped with an EDS Energy 200 and a Pentafet detector (Oxford
191 Instruments). Operating conditions were 15 kV accelerating voltage, and a beam current of 2.68 nA.
192 Quantitative data (with spot sizes of 2 μm and 15 μm in diameter, for minerals and glasses
193 respectively) were obtained and processed using the Microanalysis Suite Issue 12, INCA (Suite
194 version 4.01). Analyses were corrected for background, drift, mass absorption and secondary
195 fluorescence by using natural and synthetic standards. The relative errors are within 2% for most of
196 major elements and may go up to 10% for minor elements (with concentrations < 1.00 wt %).
197 Bulk-rock compositions were acquired by inductively coupled plasma mass spectrometry (ICP-MS)
198 analysis by ALS Chemex, Sevilla, Spain. Precision of analyzed major elements are better than
199 ±0.2% for SiO_2, and ± 0.1% for the other oxides (with the exception of MnO and P_2O_5 which show
200 errors of ca. ± 0.02%).

201

202 **Background Petrology**

203 We will briefly review the petrography of the lavas and the juvenile tephra erupted during 2002-
204 2003 and 2007. The reader may refer to Landi *et al.* (2006; 2009), Cigolini *et al.* (2008), Métrich *et*
205 *al.* (2001; 2005; 2010) and Bertagnini *et al.* (2003; 2008) for detailed descriptions.
206 *Lavas and scorias* erupted during the last two major eruptions (2002-2003 and 2007) are
207 shoshonitic basalts with crystallinity up to 35-45% modal, consisting of diopsidic clinopyroxene
208 (salite-augite), plagioclase and minor olivine on an interstitial glassy matrix (Fig. 3a; 3b).
209 Groundmass microlites consist essentially of plagioclase and clinopyroxene. Scorias are slightly
210 richer in SiO_2 and alkali when compared to the pumices ejected during both paroxysmal explosions.
211 *Basaltic pumices* have crystallinity <10% and consist of the above phases, with higher bulk MgO

(Mg# 0.55-0.60) and CaO contents, whereas K_2O is lower (2<wt %). Interstitial glass compositions are normally more evolved then those of the whole rock. *Melt inclusions* found within olivine crystals of the pumices are more primitive (with SiO_2 ranging between 45.6 and 49.4 wt % and Mg# ranging from 0.55 to 0.64). Some of these are richer in CaO and show lower alumina contents and are named *ultracalcic primitive melts*. These features have been ascribed by Pichavant *et al.* (2009) to crystal dissolution–reaction-mixing (DRM; cf., Danyushevsky *et al.*, 2004) of earlier fractionated clinopyroxene.

Fig. 3

Métrich *et al.* (2001; 2005; 2010) and Bertagnini *et al.* (2003; 2008), investigated in details primitive melt inclusions in olivine of the golden pumices. These contained 2-3.7 wt% H_2O and 700-1900 p.p.m. CO_2. They suggest the primitive gas-rich shoshonitic, or high-K basalt, is residing within the middle-lower part of the reservoir and during its ascent and storage, in a subsidiary chamber, undergoes decompression-driven crystallisation leading to the formation of a crystal-richer magma batch. The ejected materials of this kind are lapilli and scoria bombs produced during the typically “mild and persistent” Strombolian activity. However, the undegassed primitive magma is stored at deeper levels and is solely erupted during paroxysmal explosions with the ejection of the “golden pumices”. According to the cited authors, mingling and interactions of dark-coloured and crystal-rich scoria with golden-coloured crystal-poor pumice normally occur during major violent explosions (e.g., Francalanci *et al.* 1999*;* Métrich *et al.* 2001; 2005; Landi *et al.* 2004).

Fig. 4 and Table 1

In Fig. 4 we report a summary of petrochemical data onto the K_2O vs. SiO_2 diagram of Peccerillo & Taylor (1976) that shows the variability of the erupted materials. The selected analyses of the erupted products and melt inclusions are shown in Table 1.

Recently, Di Carlo *et al.* (2006) investigated phase relationships in melts of Stromboli golden pumices by selecting a sample named PST 9, that represents the less evolve pumice in the dataset. Experimental runs were carried out at temperatures of 1175-1050°C and pressures comprised between 400 to 50 MPa for variable H_2O contents (5.5-1.2 wt %) and oxygen fugacities (within 2 log units above the Ni-NiO buffer). According to their results a diopsidic pyroxene is a liquidus phase from 400 MPa to 150 MPa within the temperature range of 1175-1150°C. This phase is followed by olivine eventually crystallising with pyroxene and plagioclase, ± Fe-Ti oxide at lower P-T regimes. This is basically consistent with the cooling experiments of Conte *et al.* (2006) performed at 1 atm on somehow similar bulk compositions.

Di Carlo *et al.* (2006) experimentally confirmed that the magma type typical of the "golden pumices" is an undegassed melt that, undergoing decompression, did not extensively crystallise prior its ejection. Conversely, lava and scorias erupted during mild strombolian activity represent a degassed magma that underwent a larger degree of crystallisation at lower pressure regimes.

More recently, Pichavant *et al.* (2009) performed additional experiments on PST9 from Stromboli volcano under variable H_2O and CO_2 concentrations. Experimental fluids coexisting with primitive melts range from CO_2 rich (X_{H_2O} ~ 0.2) at 400 MPa to CO_2 poor (X_{H_2O} ~ 0.8) at 100 MPa. It was found that clinopyroxene is the liquidus phase in all high pressure experiments, either under hydrous or anhydrous conditions. In addition, at 0.1 MPa at temperatures of 1190 °C clinopyroxene and Mg-olivine appear together on the liquidus, being indicative of the onset of a cotectic relationship during decompression. The occurrence of this relationship was already established, for the assemblages of the golden pumices, by Cigolini *et al.* (2008) who found nearly constant olivine-

clinopyroxene K_D^{ol-cpx} values (based on the Fe^{2+}-Mg^{2+} exchange) in the natural assemblages (ranging 0.5 ±0.06).

Stromboli fluids

It is generally accepted that melting processes at subduction zones are generally controlled by water and carbon dioxide concentrations (e.g. Wyllie, 1979; Yoder, 1969; Mysen & Boettcher, 1975a; 1975b). Indeed, these gases play a crucial role in most magmatic processes and their abundance has a direct influence on phase stabilities and crystal-melt-gas equilibria. In addition, gas exsolution during decompression substantially controls magma ascent and fragmentation processes. However, beside these, some other minor fluid phases play a considerable role as well. Among these, sulphur degassing is a key factor in decoding volcanic activity and magma dynamics in volcanic reservoirs. A cross check between the S related petrologic method and plume SO_2 emissions is crucial for detecting magma recharge within the upper part of reservoirs, and to analyse eruption processes at active volcanoes.

Métrich *et al.* (2001; 2005; 2010) and Bertagnini *et al.* (2003) analysed sulphur, chlorine and fluorine within Stromboli glasses, including primitive melt inclusions. Sulphur concentrations found within the glasses of the "degassed" Stromboli scorias range from 170 to 250 p.p.m., whereas in primitive melt inclusions is comprised between 1200 and 2500 p.p.m.. Within the matrix glasses of porphyritic scorias, chlorine ranges from 1150 to 1270 p.p.m., while in the olivine-melt-inclusions is slightly higher, being comprised between 1500 and 2200 p.p.m.. Fluorine is rather variable: within scorias and pumices ranges from 780 to about 1050 p.p.m., whereas in primitive melt inclusions is somehow higher (960-1360 p.p.m.). Métrich *et al.* (2010) found that S is positively correlated with pressure, whereas Cl and F contents do not show appreciable variations with pressure changes. In particular, they suggested that SO_2 is released at pressures of about 170 MPa or lower. We will later discuss how sulphur degassing may give important information on magma volumes involved in recharge processes and magma chamber dynamics.

Stromboli fluids are also carefully monitored in volcano surveillance. Radon emissions (e.g., Cigolini *et al.*, 2009; 2013; Laiolo *et al.*, 2012) and CO_2 fluxes are automatically measured (Rizzo *et al.*, 2009; Carapezza *et al.*, 2009). Carbon dioxide SO_2 and H_2S are also continuously detected in the volcanic plume by means of a multigas analyzer (Aiuppa *et al.*, 2005; 2009) and FTIR (La Spina *et al.*, 2013). In addition, SO_2 is also carefully monitored by systematic COSPEC measurements (Burton *et al.*, 2009). We will later consider some key issues that arise from the analyses of the collected SO_2 timeseries when compared to eruption discharge rates.

In this section, we prefer to briefly review gas compositions sampled at the summit of Stromboli. The data are few but quite significant. Following the early measurements of Tazieff and Tonani (1963), gases released at Stromboli summit fumaroles were analysed by Carapezza & Federico (2000) and by Finizola *et al.* (2003). Geothermometric estimates on the gases collected by Finizola *et al.* (2003), obtained by means of the CO_2-CH_4-CO geothermometer (Chiodini & Cioni 1989), give equilibration temperatures of 265-275°C. These temperatures are in good agreement with those obtained graphically on the diagram $\log(H_2O/H_2)+\log(CO/CO_2)$ vs. $3\log(CO/CO_2)+\log(CO/CH_4)$ constructed by Chiodini & Marini (1998) that classify these fluids as superheated vapors. Thus, these gases have essentially an hydrothermal origin (with X_{H_2O} approaching 0.90).

However, Martini *et al.* (1996) reported two gas compositions obtained on samples collected by M. Ripepe within a fracture located at the rim of the NE summit crater. These gases have definitely higher X_{CO2} concentrations, ranging from 0.33 up to 0.73, and their sampling temperatures were 410 and 190°C. Noticeably, FTIR data reported by Burton *et al.* (2007) found that during the typical strombolian explosions X_{CO_2} fractions are normally 0.33, and X_{H_2O} may be as high as 0.64. Conversely, during quiescent degassing (or gas puffing) the above reach 0.13 and 0.83, respectively (the rest, up to 1, being essentially SO_2 and HCl in equal proportions).

Equilibrium assemblages in primitive melts

Natural assemblages are complex systems. However, we may use experimental data and computer modelling (e.g., MELTS) to better constrain P-T-*X* variability. Both these approaches are based on the fact that equilibrium conditions are reached, and rule the evolution of the system. Unfortunately, the effects of volatile concentrations on phase stabilities are still inadequately known (such as the stability field of plagioclase and clinopyroxene in function of changing hydrous conditions, cf. Yoder, 1969; Kushiro, 1979; Métrich *et al.*, 2001). In this section, we will analyse the available data on Stromboli to identify equilibrium assemblages by using standard consolidated methods, normally applied in igneous petrology.

We thus explored the equilibrium conditions of Stromboli primitive basalts by analyzing minerochemical data and melts compositions in terms of distribution coefficients.

Among these, we first consider the olivine-liquid distribution coefficient ($K_D^{ol-liq} = X_{Fe}^{ol} X_{Mg}^{liq} / X_{Mg}^{ol} X_{Fe}^{liq}$). According to Roeder & Emslie (1970), equilibrium conditions are satisfied for a value of 0.33 in this parameter. However, Kamenetsky et al. (1998) has suggested that this parameter may range from 0.27 to 0.29 in alkaline mafic magmas. According to Putirka (2008), the appropriate K_D^{ol-liq} values for basaltic magmas is 0.299 (±0.05). For Stromboli basalts, Métrich & Clocchiatti (1996) and Di Carlo *et al.* (2006) constrain the olivine-melt Mg-Fe distribution coefficient at 0.29 for equilibrium conditions. Thus a melt with a Mg-number (Mg#) of 0.58 (i.e., one of the more mafic within the melt inclusions) will be in equilibrium with an olivine Fo_{83}. The latter authors suggest that the Mg-Fe partition coefficient, for clinopyroxene-liquid equilibrium $K_D^{cpx-liq} = X_{Fe}^{cpx} X_{Mg}^{liq} / X_{Mg}^{cpx} X_{Fe}^{liq}$, is constrained to about 0.31 (±0.06) according to their experimental data. However, Putirka (2008) emphasised that the best estimate for this parameter is 0.28 (±0.08) over a wide range of magma compositions.

Concerning the plagioclase-melt equilibrium, we considered a Ca-Na exchange between the two phases, $K_D^{pl-liq} = X_{Ab}^{pl} X_{AlO1.5}^{liq} X_{CaO}^{liq} / X_{An}^{pl} X_{SiO2}^{liq} X_{NaO0.5}^{liq}$ accepting a value of 0.27 ±0.05 (cf. Putirka,

337 2008). In Table 2 we report a selection of representative mineral phases of the erupted products that
338 are compatible with their coexisting melts and satisfy the above partitions coefficients.
339
340 **Table 2**
341
342 An additional issue is plagioclase stability. First, petrography shows that plagioclase (locally
343 euhedral) is an "ubiquitous" phase in all the erupted pumices. Second, Di Carlo *et al.* (2006) report
344 a high-pressure run (at 400 MPa, 1100°C and 2.3 H_2O wt%) of a pumiceous melt (PST9) where
345 plagioclase crystallises. Five other experimental runs at the same temperature, lower pressure and
346 lower H_2O contents define the plagioclase stability field. In the experimental works of Pichavant *et*
347 *al.* (2009) plagioclase does not crystallise since they were performed at higher temperature
348 (T>1150°C). However, starting from the same melt composition, Conte *et al.* (2006) found that
349 plagioclase is a crystallising phase in their experiments at atmospheric pressure and temperature
350 below the 1150°C. By testing the crystallisation Stromboli primitive basalts (including sample
351 PST9) with the computer code MELTS (Ghiorso & Sack 1995), we found that clinopyroxene is
352 liquidus phase above 250 MPa and 1175°C, whereas olivine becomes a liquidus phase together with
353 clinopyroxene at lower pressure, and plagioclase would appear on the liquidus below 50 MPa for
354 temperatures approaching 1100°C.
355
356 **Fig. 5**
357
358 In order to assess the role of plagioclase during the crystallisation of Stromboli primitive basalts we
359 analyzed the data by means of Pearce element ratios (Pearce & Stanley, 1991). These can be used to
360 constrain the fractionating mineral phases within a given magma (cf. Russell & Nicholls, 1988). We
361 thus plotted the data (ours plus those in literature) on the (2Ca+3Na)/K vs. Si/K diagram (Fig. 5a).
362 A slope approaching to 1 indicates a pair removal. In our case the calculated slope is 0.90 (with a

correlation coefficient of 0.85), thus suggesting the fractionation of both phases (clinopyroxene and plagioclase). Fig. 5b with (2Ca+Na)/K vs. Al/K indicates a higher proportion of clinopyroxene removal relative to plagioclase (0.60 to 0.40, respectively) (Fig. 5b). Finally, the 2Na/K vs. Al/K diagram allow us to estimate that an average plagioclase of composition of about An_{82-76} was involved in the fractionation of Stromboli primitive basalts (Fig. 5c). Whereas a labradoritic plagioclase (An_{67-62}) is involved in the crystallization of evolved melts. In both cases their values satisfy K_D^{pl-liq} constraints (0.23±0.01) and are consistent with the petrography of lavas and scoriaceous materials.

Geothermometry and Geobarometry

In this section we will first apply classical geothermometers and geobarometers to estimate the P-T regimes of Stromboli primitive melts. We will then refine our estimates by introducing a grid of selected reactions that will help us to further constrain equilibrium regimes for selected mineral-melt compositions. Finally, we synthesise our results and discuss them to better infer the extension of Stromboli magma reservoir.

First, the results obtained by systematically applying classical thermobarometers are reported in Table 3 (see the footnotes of this table relative uncertainties). Hydrous melt inclusions and bulk pumices with H_2O contents comprised between 2-3 wt %, show equilibration temperatures for their liquids in the range of 1100-1220°C. Lower values are obtained by using the algorithm of Sisson & Grove (1993), being constrained to 1100-1160°C. With the exception of the results obtained by applying the Putirka (2008) liquid thermometer (leading to temperatures of 1145-1185°C), other geothermometers substantially overlap, in the range of approximately 1160-1220°C.

Olivine-liquid geothermometers only partly overlap. Higher temperatures are obtained by using the one proposed by Beattie (1993) leading to temperatures of 1150-1220°C. The results obtained by calculating the Sisson & Grove (1993) and Putirka (2008) geothermometers are basically consistent

388 at lower temperatures (1100 ± 30 °C), whereas in the higher temperature ranges lead to about
389 1150°C and 1190°C, respectively (Table 3).
390
391 **Table 3**
392
393 The geothermometers that use clinopyroxene-liquid equilibria are essentially those proposed by
394 Putirka *et al.* (2003) and Putirka (2008; equations 32d, 33, 34), and practically overlap in the
395 temperature range of 1110-1220°C (Table 3). Finally, the clinopyroxene-liquid barometers
396 proposed by the latter author indentify rather variable equilibration pressures. Among these, the
397 most coherent with previous estimates (Métrich *et al.*, 2001; 2005; 2010; Bertagnini *et al.*, 2003 and
398 Cigolini *et al.*, 2008) are those obtained by applying his equation (30) of Putirka (2008), leading to
399 pressures of 170-360 MPa for the melt inclusions, and 210-290 MPa for the bulk pumices,
400 respectively. Unfortunately, Putirka's geobarometers show a good degree of uncertainty (see the
401 footnote of Table 3), so we had to find more reliable geobarometers.
402
403 ***A grid of selected reactions***
404 Thus, in order to minimize uncertainties related to the applications of the classical
405 thermobarometers treated above, we used a grid of selected reactions which involve solid-melt
406 equilibria to better constrain the P-T regimes that adequately describe our system.
407 These are the following:
408
409 $Mg_2SiO_4 + SiO_2 = Mg_2Si_2O_6$ (1)
410 Fo liq CEn
411
412 $CaMgSi_2O_6 = 1/2\ SiO_2 + 1/2Mg_2SiO_4 + CaSiO_3$ (2)
413 Di liq Fo (liq) Wo (liq)
414

$$CaAl_2Si_2O_8 + 2Mg_2SiO_4 + SiO_2 = 2Mg_2Si_2O_6 + CaAl_2SiO_6 \quad (3)$$
An Fo liq CEn CaTs

$$CaAl_2Si_2O_8 = CaAl_2SiO_6 + SiO_2 \quad (4)$$
An CaTs liq

Abbreviations below reaction components are: Fo – forsterite; CEn – clinoenstatite; Di – diospide; Wo – wollastonite; An – anorthite; CaTs – Ca-Tschermakite. Abbreviated mineral phases are solid, unless otherwise indicated (as liquid, liq)

Reactions (1) and (2) have been used to estimate P-T regimes for the coexistence of olivine and pyroxene, and to identify the upper stability field of diopsidic pyroxene in hydrous Stromboli basaltic melts. However, the use of melt components in thermodynamic calculations has the advantage of considering the water contents in the melt phase. In addition, reaction (3) is a rather efficient geobarometer (e.g., Laiolo and Cigolini 2006; Cigolini et al., 2008) in the stability field of bytownitic plagioclase and ferromagnesian phases consistent with the mineral assemblage found in Stromboli pumices. Finally, reaction (4) is typical of the low pressure assemblage where a labradoritic plagioclase is coexisting with augite and a differentiated groundmass melt under nearly anhydrous conditions (*ca*. 0.5 wt% H_2O, cf. Stevenson & Blake 1998). Regarding this reaction, we will discuss the results of obtained in our previous study (Cigolini *et al.*, 2008). The degree of oxidation of the melt has been retrieved, following Kress & Carmichael (1991), from the Ni-NiO buffer of Hübner & Sato (1970), appropriate for Stromboli magma (cf., Laiolo & Cigolini 2006), taking into account the effect of pressure (in the light of the data of Robie *et al.*, 1979).

The Gibbs free energy for a generic *i* reaction is represented by

$$\Delta G_0^{P,T} = \Delta G_0^{1,T} + RT \ln K_i + \int_1^P \Delta V dP \quad (5)$$

where $\Delta G_0^{1,T}$ is the Gibbs free energy for the reaction calculated at 1 bar and at the temperature of interest (*T*) by using the data of Berman (1988; cf. his Table 2, 3, and 4 p. 458-463) together with those of Richet *et al*. (1982) for amorphous silica, and those of Ghiorso & Sack (1995) for other melt components (Table A1, p. 209 of their work). A synopsis of used thermodynamic data is reported in Table A2 of Cigolini *et al.* (2008). *R* is the gas constant and K_i is the equilibrium constant for the *i* reaction considered, which may be calculated, knowing the chemical compositions of the analysed phases, from the appropriate solution models. The last term is the difference of the molar volumes of the reactants minus the products of the reaction integrated within the given pressure range. This can be solved numerically at given equilibrium conditions by using the cited data of Berman (1988), and those listed by Ghiorso & Sack (1995) for the melt components, that include thermal expansion and compressibility.

In the studied reactions, activities for olivine, pyroxene and plagioclase were calculated according to the solution models of Sack & Ghiorso (1989), Gasparik (1984; 1990) and Newton *et al.* (1980), respectively. Activities of melt components were obtained according to the regular solution model of Ghiorso & Sack (1995) and change with the water content in the melt phase. The solution of the above equation has been obtained numerically, by minimizing the free energy $\Delta G_0^{P,T}$ (that goes to zero at equilibrium conditions) by fixing a given value of T and calculating P (or vice versa). The same procedure has been applied to the set of the above reactions. A summary for the equilibrium constants is given in Table 4. Melt compositions and mineral phases used in calculations are summarised in Table 1 and Table 2, respectively.

Table 4

The reference melt for reactions (1) and (2) are the selected melt inclusions found within the olivines of ejected pumices (reported by Métrich *et al.*, 2001; 2005; 2010; and Bertagnini *et al.*, 2003) and identified as a primitive Stromboli basalts. Reaction (3) defines equilibrium conditions of

the golden pumices (bulk composition). Reference data are given in Table 1, whereas the selected equilibrium mineral phases are summarized in Table 2.

In the APPENDIX we report the thermodynamic solutions for the for melt inclusions (Tables A1 and A2) and the bulk pumice (Table A3). The same data have been used to construct Figure 6.

Fig. 6

In particular, Stromboli primitive melts (Mg# 0.57 and CaO/Al_2O_3 0.73) are in equilibrium with a Fo-rich olivine (Fo_{84-80}) and a diopsidic pyroxene ($Wo_{44-48}En_{43-48}Fs_{6-9}$) at temperatures of 1140-1170 °C and pressures of 260 (±60) and 440 (±70) MPa for water concentrations ranging 2-4 wt%, respectively. More realistic best solutions are those for water being comprised between 2-3 wt%, giving temperatures of 1150-1160 °C and pressures of **280-340 MPa**. Similar reasoning for the Ca-rich melts (Mg# 0.63 and CaO/Al_2O_3 0.93) will give higher equilibration temperatures and lower pressures, with best solutions of 1160-1180 °C and pressures of 180 (±70) and 280 (±90) MPa with water contents of 2-3 wt%. The olivine in equilibrium with the ultracalcic melts are Fo_{88-90}. Finally, equilibration P-T regimes for the golden pumices, given by the coexistence of the above mineral phases and a bytownitic plagioclase (An_{82-78}) will constrain temperatures at 1120-1140 °C and pressures of 190 (±40) and 170 (±50) MPa for similar water contents (2-3 wt%).

Thermobarometric estimates for the upper part of the chamber were obtained by considering the equilibrium of phenocristic rims with the coexisting groundmass melt (and the reader may refer to Cigolini *et al.*, 2008 for details). These data have been used, together with the above, to construct Fig. 7.

Thermobarometry of Melt Inclusions

Better constraining the P-T regimes of melts coexisting with volatiles is a key factor for decoding in-chamber magma dynamics (e.g., Witham, 2011a; Métrich *et al.*, 2011; Witham, 2011b).

In our earlier paper (Cigolini *et al.*, 2008) we calculated mineral-melt equilibria for the melt inclusions reported by Métrich *et al.* (2001) according to the following reaction

$$\underset{\text{Fo}}{Mg_2SiO_4} = \underset{\text{Fo (liq)}}{Mg_2SiO_4} \quad (6)$$

By summing up the above with reaction (2), we obtain the following:

$$\underset{\text{Di}}{CaMgSi_2O_6} + \underset{\text{Fo}}{Mg_2SiO_4} = 1/2\ \underset{\text{liq}}{SiO_2} + 3/2\underset{\text{Fo (liq)}}{Mg_2SiO_4} + \underset{\text{Wo (liq)}}{CaSiO_3} \quad (7)$$

which is representative of the olivine-clinopyroxene cotectic relationship. According to Pichavant *et al.* (2009) such a relationship is critical for assessing equilibrium conditions in Stromboli basalt. We therefore extended our thermodynamic calculations by taking into account a more comprehensive data set (including the data of Bertagnini *et al.*, 2003; Métrich *et al.*, 2001; 2005; 2010). In Table 5 we report the selected melts together with the appropriate clinopyroxene compositions that satisfy the $K_D^{Cpx-liq}$ requirements of Putirka (2008).

Table 5 and Table 6

In this section the notations $X^m_{H_2O}$ and $X^m_{CO_2}$ refer to the fractions of water and carbon dioxide in the binary mixture dissolved in the melt under saturation conditions ($X^m=X^V$): so that $X^m_{H_2O} + X^m_{CO_2} = 1$. The above equilibrium can be solved for *P, T,* $X^m_{H_2O}$ and $X^m_{CO_2}$ for the given fluid concentrations (in wt% as input data) by minimising the free energy of the above reaction and solving simultaneously the solubility equations of Dixon & Stolper (1995) and Dixon (1997). The insertion of the molar

520 heat of solution for H_2O in the melt (determined on albite melt by Silver & Stolper 1985) for
521 polythermal calculations has been shown to be negligible with respect to free energy minimization.
522 In other words, we are first solving thermodynamically the required thermodynamic conditions
523 along a Clausius-Clapeyron equation representative of minerals-melt equilibrium. The solution is
524 then found for the P-T conditions that satisfy the observed volatiles concentrations according to the
525 model of Dixon for alkaline basalts (Dixon, 1997). We trust that this approach is more reliable
526 because we are analyzing a three phase system (solids, melt and gas) that substantially improves the
527 commonly used two phase solubility models (e.g., Newman & Lowenstern 2002; Papale *et al.*,
528 2006).
529 In Table 6 we report the solutions for the above reaction for selected melts in equilibrium with the
530 chosen clinopyroxene compositions. These data indicate that primitive melt inclusions are in
531 equilibrium with ferromagnesian phases at pressures between 3.3 and 2 kbar and temperatures
532 ranging from about 1150 to 1200°C (with average values of about 1170°C, and only one melt
533 inclusion slightly above 1200°C). It is interesting to notice that calculated $X^{m}_{CO_2}$ values range from
534 0.6 to 0.76. These estimates are in good agreement with the previous ones obtained by the models
535 of Newman & Lowenstern (2002) and Papale *et al.* (2006) models (e.g., Métrich *et al.*, 2005; 2010;
536 Bertagnini *et al.*, 2003). However, similar calculations performed by mean of reaction (6) for the
537 primitive melt inclusions lead to similar pressures but unrealistically higher temperatures (nearly
538 20-25°C higher, being incompatible with experimental data).
539 Notably, melt inclusions in scorias equilibrate with Fe-richer olivine (ca. Fo_{70}) and an augitic
540 pyroxene at pressures of 60-100 MPa and temperatures ranging from 1120 to 1145°C (Table 7 and
541 Table 8). However, calculated $X^{m}_{CO_2}$ are much higher (being comprised between 0.79 and 0.98)
542 since the water contents of these melt inclusions are very low (and substantially they are indicative
543 of a degassed magma). In this case also the thermodynamic solutions of reaction (6) give similar
544 pressure ranges as well, but considerable higher temperatures (up to 60°C) which are definitely

unrealistic. Therefore a cotectic relationship defined by reaction (7) is by far more appropriate for identifying solid-melt-fluid equilibration regimes in Stromboli basalts.

Table 7 and Table 8

Summary of Thermobarometry

Our best estimates suggest primitive hydrous melts preserved as melt inclusions in olivine (with 2.3-3.8 wt% of H2O) are in equilibrium with forsteritic olivine and a diopsidic clinopyroxene at pressures of 200-340 MPa pressure and temperatures of 1150-1200°C. Average data of calculations on melt inclusions are 260 (±47) MPa and temperatures of 1170 (±17) °C. These regimes are representative of the base of the chamber, where the ferromagnesian phases may crystallise and cumulate (see Laiolo & Cigolini 2006; Cigolini et al., 2008). However, slightly more evolved melts, typical of the *golden pumices* (with 2-3 wt% H_2O), are in equilibrium with Ca-pyroxene, forsteritic olivine and anorthitic plagioclase at 150–220 MPa and temperatures approaching 1120-1150°C. These materials likely represent the middle and main part of the chamber.

In turn, thermobarometric estimates for the upper part of the chamber were obtained by Cigolini *et al.* (2008) by considering the equilibrium of phenocristic rims with coexisting groundmass melts (with Mg# of 0.20-0.25). The upper part of the chamber where the reservoir is connected with the conduit is confined at 140-120 MPa for temperatures approaching 1100°C (which is the measured effusion temperature for the lavas). Evolved melt inclusions in Fe-richer olivine (ca. Fo_{70}) of the scorias show average equilibration pressures of 78 (±20) MPa, and temperatures 1138 (±14)°C, being indicative of crystallisation within the conduit or its root-zone that reaches the upper part of the chamber.

However, Stromboli magmas originate above the slab at an approximate depth of about 100 km (Schiavi *et al.*, 2012). From this depth melts will progressively migrate to upper levels and interact

570 with the ultramafic materials at depths of 34-24 km were temperatures reach 1200-1250°C (Cigolini
571 *et al.*, 2008). In this region, the magma is percolating through the wallrocks of the LVZ and may
572 converge into a feeder dyke that crosscuts the Moho. On their way to the surface, basaltic magmas
573 may decompress along a steep adiabatic and/or isothermal curve crosscutting the stability field of
574 diopside thus entering the liquidus field and generating ultracalcic melt inclusions. To better
575 visualize this process we compiled summary of the mineral stabilities in Stromboli basalts (Fig. 7)
576 in the light of the previously cited experimental data and the above equilibria, together with those
577 reported by Cigolini et al. (2008) for the low pressure assemblage. The possible decompressional *P-*
578 *T* path (at higher pressures) for explaining the origin of the ultracalcic melts is also plotted (upper
579 path in Fig. 7). During decompression the magma path will cross the clinopyroxene stability field
580 and enter the liquidus field. The earlier crystallized diopside is destabilized and will react with the
581 melt leading to the formation of ultracalcic melts. Subsequent cooling associated with moderate
582 decompression, and/or at nearly isobaric conditions, will lead to crystallization of the
583 ferromagnesian phases again. This scenario is basically supporting the hypothesis of Pichavant *et*
584 *al.* (2009) that suggest that Ca-rich melts are related to crystal dissolution–reaction-mixing (DRM;
585 cf., Danyushevsky *et al.*, 2004) of earlier fractionated clinopyroxene.

586 **Fig. 7**

587 Once the magma has entered the chamber, it will be stored undergoing fractionation and degassing.
588 Further decompression and cooling, accompanied by crystallisation of clinopyroxene followed by
589 Fe-richer olivine and plagioclase, will lead the basaltic magmas typical of scorias and lavas (Fig. 7).
590 The most active part of the chamber is its axial sector, where the magma column, consisting of fresh
591 magma of lower density and viscosity, will progressively migrate upward and degas before being
592 erupted (cf., Cigolini et al., 2008).

593 **Geophysical constraints on magma chamber volumes: inference from SO_2 degassing**

594 ***SO_2 flux and magma degassing rate***

595 Stromboli volcano is known for its remarkably steady state magma supply rates, as well as for the
596 continuous degassing rates associated with magma rise within the shallow magmatic system (Allard
597 et al., 1994). Recent SO_2 fluxes, representative of time-averaged sulphur emissions during
598 strombolian activity, were estimated to be approximately 150-200 t day^{-1} (Burton *et al.*, 2007;
599 2009). However, the February–April 2007 eruption was accompanied by an "exceptional" (above
600 normal) degassing rate (Fig. 8) with mean SO_2 emissions of *ca.* 620 t day^{-1}, i.e. 3-4 times higher
601 than those occurring during the typical strombolian activity (Burton *et al.* 2009). Although higher
602 than normal, the volume of magma degassed during the 35 days of lava effusion (February-April
603 2007), estimated from the SO_2 flux (~2 x 10^6 m^3 dense rock equivalent, d.r.e., Burton *et al.*, 2009)
604 was drastically lower than the volume of erupted lava (~8 x 10^6 m^3 d.r.e.; Calvari *et al.*, 2010,
605 Marsella *et al.*, 2009). Burton *et al.* (2009) suggested that such an unbalance could be reconciled by
606 considering an unrealistically high vesicularity of the 2007 lavas (>60%) or, better, by the assuming
607 that the most of the erupted magma volume (nearly 6 x 10^6 m^3) was already degassed when it was
608 erupted. Since, lava vesicularity at Stromboli is typically comprised between 16 and 32% (Fornaciai
609 *et al.*, 2009), the effusion of a large volume of degassed magma seems to be the case (due to the
610 drainage of a shallow plumbing system where the magma undergoes degassing). This may explain
611 the deficit in sulphur degassing observed during the February 2007 effusive eruption.
612 However, the long term record of sulphur output (Burton *et al.*, 2009) reveals that high values of
613 SO_2 flux persisted for several months after the ceasing of the effusive phase (see Fig. 8). In
614 particular, the trend shown in Fig. 8 suggests that the period of anomalous degassing (February to
615 October 2007) was characterised by an gradual decline of the SO_2 flux, which decreased to pre-
616 eruptive levels (i.e 150 t day^{-1}; Burton *et al.*, 2009) only in October 2007, about 200 days after the
617 end of the lava effusion.
618 The sulphur output data shown in Fig. 8 allow us apply the petrologic method (cf., Palma *et al.*,
619 2011) in order to estimate the magma degassing rate (Q_{degas}) of Stromboli during the period of
620 anomalous degassing (i.e. February to October 2007). In fact, the magma degassing rates (in terms

621 of the volumetric flux of magma undergoing sulphur degassing; m^3 s^{-1}) can be derived by the
622 estimates of SO_2 flux (ϕ_{SO_2}) and by the measurements of sulphur concentration in melt inclusions
623 (found within olivine phenocrysts) and in the interstitial glasses of the erupted materials (cf.
624 Kazahaya et al., 1994; Gerlach et al., 1996). To retrieve the magma degassing rates (Q_{degas}), we may
625 write this relationship as:

626 $$Q_{\deg as} = 10^2 \frac{M_S}{M_{SO_2}} \frac{\phi_{SO_2}}{\Delta S} \frac{1}{\rho_M} \qquad (8)$$

627 where M_S and M_{SO_2} (both in g/mol) are the molecular mass of sulphur and sulphur dioxide,
628 respectively. The ϕ_{SO_2} (kg/s) is the sulphur degassing rate and ΔS (wt%) represents the total
629 outgassed sulphur, calculated as $\Delta S = S_{mi}(1-x_{mi}) - S_{ig}(1-x_{ig})$, where S_{mi} (wt%) and S_{ig} (wt%) are
630 respectively the sulphur concentration in the melt inclusions and in the interstitial glass, and x_{mi} and
631 x_{ig} are, respectively, the crystals during the trapping of the melt inclusions (assumed to be zero) and
632 the crystals content in the matrix, as fraction. Moreover, ρ_M represents the bulk density of the
633 magma entering in the degassing zone. Q_{degas} was then calculated by taking into account a S content
634 of 0.24 wt% and 0.04 wt% in the primitive magma and in the scoria interstitial glasses, respectively
635 (cf. Bertagnini et al., 2003) and considering x_{ig} = 0.3 (being consistent with Stevenson & Blake,
636 1998).
637 It is generally accepted that at Stromboli volcano, the magma degassing rate (Q_{degas}) provides
638 constraints for the magma supply rate (Q_{in}) or rather for the rate at which volatile-rich aphyric
639 basalt (LP magma) enters in the shallow plumbing system where sulphur degassing takes place (Allard et
640 al., 1994, 2008). Hence, the trend drawn by Q_{degas} (Fig. 8) can be regarded as the flux of magma
641 rising from a deep portion of the plumbing system (hereby defined as R_{deep}), where the Low
642 Porphyritic (LP) magma resides with little crystallisation and degassing, to a shallowest storage
643 zone (defined as $R_{shallow}$) where gas-melt separation occurs, thus promoting the steady strombolian
644 activity (Allard, 2008).

Thus, the magma supply (degassing) rate shown in Fig. 8 is likely representative of the LP magma flux that entered the degassing cell of Stromboli during and after the 2007 effusive eruption. As shown in Fig. 8 this magma flux see the contribution of two combined processes: *(i)* the constant supply of LP magma typical of the steady state regime of Stromboli ($Q_{in\text{-}steady}$) and *(ii)* the anomalous (in excess) supply of LP magma entered in the degassing zone during and after an effusive phase ($Q_{in\text{-}ex}$). Notably, the whole magma supply rate affected by degassing Q_{degas} (being equal to $Q_{in\ steady} + Q_{in\ ex}$) describes a clear exponential trend (Fig. 8) that can be described by:

$$Q_{\text{deg}\,as} = Q^{0}_{in-ex} \cdot \left[\exp\left(-t/\tau\right)\right] + Q_{in-steady} \qquad (9)$$

where Q^{0}_{in-ex} is the initial excess of magma supply (i.e., related to the effusive phase) and τ is the calculated decay constant.

The coefficients retrieved from the best-fit regression indicates an initial Q^{0}_{in-ex} of 0.73 m^3 s^{-1}, a decay constant (τ) of 82.5 days and a steady magma supply ($Q_{in-steady}$) equal to 0.1 m^3 sec^{-1}**,** the latter being in good agreement with the typical magma degassing rate of Stromboli (Allard *et al.*, 2008; Tamburello *et al.*, 2012). It follows that the integration of the curve plotted in Fig. 8 provides the cumulative volume *LP* magma transferred from R_{deep} to $R_{shallow}$ during the anomalous SO_2 flux (approximately 230 days). This volume is thus obtained by summing the volume of magma supplied at constant rate ($V_{in\text{-}steady} = Q_{in-steady}$ x 230 days = ~2 x 10^6 m^3) and the volume of magma in excess, obtained by integrating $Q_{in\text{-}ex}$ ($V_{in\text{-}ex} = Q^{0}_{in-ex}\,\tau$ =~5.2 x 10^6 m^3). As a whole these calculations brings the total volume of the LP magma that entered the shallow reservoir ($V_{in} = V_{in\text{-}ex} + V_{in\text{-}steady}$) to ~7.2 x 10^6 m^3 . This value is surprisingly similar to the volume erupted during the 35 days of effusion (V_{erupt}~8 x 10^6 m^3 d.r.e. between 27 February and 4 April 2007) and implies that $R_{shallow}$ was almost replenished in about 230 days. In addition it is remarkable to note that these results are in good agreement with the size of the degassing cell of Stromboli inferred by Allard *et al.* (2008; 12 (±3) x 10^6 m^3), as well as with the maximum residence time of magma in the

degassing cell (being around 215 days, as assessed from the ratios of short-lived radioactive daughters; Gauthier *et al.*, 2000).

Constraints on deep reservoir capacity and volume

The fact that the long term trend of $Q_{in\text{-}ex}$ leads to an overall exponential decay is intriguing, since this relationship is typical of pressurised magmatic systems and generally characterise the magma discharge during some basaltic eruption (Wadge, 1981). In the case of Stromboli we explain this behaviour by suggesting that that the LP magma, rising and entering within $R_{shallow}$, was accompanied by a slow decompression of the deeper portion of the plumbing system of Stromboli (R_{deep}). This process was slower than the one associated to lava effusion (that, in turn, has been lasting for 32 days; Bonaccorso *et al.*, 2008), and is indicative of the fact that deeper sector of the plumbing system exhibited a slow response to the pressure drop associated with lava effusion.

The exponential decline of Q after a short waxing phase is generally ascribed to the release of elastic strain accumulated either by pressurisation of the rocks surrounding the magma reservoir, or by pressurisation of the magma, or both (Wadge, 1981, Stasiuk *et al.*, 1993; Harris *et al.*, 2000, Aki & Ferrazzini, 2001; Huppert & Woods, 2002). According to these models, if the elastic strain is the sole driving force of magma, at any time *t*, the volumetric flux *Q(t)* is described by:

$$Q(t) = Q_0 \cdot \exp(-t/\tau) \qquad (10)$$

where Q_0 is initial flux and τ is the time constant of the exponential decay. By analogy with a resistor-capacitor circuit, Aki & Ferrazzini (2001) proposed that the time constant τ can be simply expressed as:

$$\tau = R_e C \qquad (11)$$

where C is the capacity of the reservoir undergoing decompression (in m^3 Pa^{-1}) and R_e, is the resistance of the "channel" (dike or conduit) to the magmatic flux (in $Pa\ s\ m^{-3}$). Therefore, high reservoir's capacity and/or high channel's resistance will produce longer time constant and slower waning phases.

By assuming that the elastic strain is accumulated either by pressurisation of both the magma and the rocks surrounding the reservoir, the capacity C can be obtained, considering wall-rock and magma compressibility (cf., Mastin *et al.*, 2008), as

$$C = \frac{\rho_M}{\rho_e}\left(\beta_R + \beta_M\right) V_R \qquad (12)$$

where ρ_M, ρ_e are the densities of magma and erupted lava, respectively, β_M is the magma compressibility, β_R is the wall-rock compressibility and V_R is the reservoir volume undergoing strain release. On the other hand the initial effusion rate Q_0 is related to the channel (conduit) resistance R_e through the following Aki & Ferrazzini (2001):

$$Q_0 = \frac{P_0}{R_e} \qquad (13)$$

where P_0 is the initial overpressure (in Pa). By integrating equation (9) it follows that a generic volume (V_{out}) transferred outside the chamber is given by

$$V_{out} = Q_0 \tau, \qquad (14)$$

or alternatively by

$$V_{out} = CP_0 \qquad (15)$$

In order to constrain the volume of the deep reservoir undergoing the strain realise, the anomalous (in excess) supply of LP magma entered in the degassing zone ($Q_{in-ex} = Q^0_{in-ex} \cdot \exp(-t/\tau)$) can be analysed in the light of the above model. In particular, by determining the initial overpressure (P_0),

717 magma compressibilities (β_M and β_R) and densities (ρ_M and ρ_e), the capacity (C) and volume (V_R) of
718 the reservoir can be constrained throughout equations (10) to (15).
719 During the onset of 2007 eruption a near instantaneous pressure drop of about 4-6 MPa was
720 transferred to the upper part of the reservoir that instantaneously decompressed (Calvari *et al.*
721 2011). At the same time, a large supply of CO_2-rich and SO_2-rich gas bubbles from the deep low
722 porphyritic (LP) sector of the reservoir (Burton *et al.*, 2009; Aiuppa *et al.*, 2010a, b), has been
723 invoked, as a consequence of depressurisation associated with lava drainage since the onset of the
724 eruption (27 February 2007; Bonaccorso *et al.*, 2008). Therefore, it is not unreasonable to assume
725 that an initial overpressure ≥ 5 MPa affected the whole plumbing system of Stromboli during the
726 beginning of the eruption. By setting P_0 = 5 - 10 MPa and by assuming that the magma volume
727 entering in the degassing zone, was substantially the one removed outside the deeper reservoir
728 ($V_{in\text{-}ex} \sim V_{out}$, recalling that is equal to 5.2 x 10^6 m^3), we estimated a capacity C roughly comprised
729 between 0.52 and 1.05 m^3 Pa^{-1} (equation 15).
730 We than calculated the variation of compressibility of primitive melts by taking into account the
731 variations in fluid contents during step-by-step decompression associated with bubble growth. Melt
732 densities (ρ_l) were calculated according to Lange & Carmichael (1990), whereas the gas-mixture
733 densities (ρ_g) were obtained by applying the Modified Redlich-Kwong (MRK) equation of
734 Holloway (1977). The quantities of water and CO_2 (in wt%) released during decompression were
735 obtained by applying the computer code VOLATILECALC of Newman & Lowenstern (2002). Thus,
736 the magma bulk density (ρ_M) and compressibility (β_M) were calculated according to Huppert and
737 Woods (2002, equations 5 and 6 of their work) that take into account crystallinity and the
738 contribution of wall-rock compressibility (β_R = 3 $^{-11}$ Pa^{-1}). The latter parameter was retrieved
739 (assuming a Poisson ratio of 0.25) from the rigidity calculated by D'Auria et al. (2006) for
740 earthquakes located in the surrounding of the top of the magma reservoir (at 4.5-6 km depth). The
741 selected melt for calculating the appropriate magma compressibility (β_M) is the average of the

analyses of melt inclusions reported in Table 5. Thus, given the magma pressure-dependent compressibility model shown in Fig. 9, we may consider that at 200 MPa (i.e., the main portion of the reservoir) the magma compressibility, β_M reaches 4^{-10} Pa^{-1}, while the wall-rock compressibility, β_R, is almost one order of magnitude less. In Table A5 we report the isothermal decompression path together with the results of our calculations. Similarly, we may assume that during its transfer from the deep to the upper part of the chamber, the magma changed its density from ρ_M = 2690 kgm^{-3} (unvesiculated magma) to ρ_e = 2480 kg m^{-3} (erupted vesiculated magma). By using equation (12), for the above calculated reservoir capacity (C= 0.52 and 1.05 m^3 Pa^{-1}), we estimated the volume of the reservoir undergoing the elastic strain release (V_R): being comprised between 1 and 2 km^3, in good agreement with the lower volume estimates of Cigolini *et al.* (2008) for the Stromboli magma chamber.

Fig. 9

Discussion and conclusions

In this contribution we have revisited the data on the last two major eruptions at Stromboli volcano and concentrated our analysis on the 2007 eruption. Our main goal was to offer a comprehensive view of the problems connected with the interpretation of the onset and evolution of these events and how their analysis may contribute to better understand the inner dynamics of this complex volcanic system. We therefore focussed our research on how volatiles contents affect solid-melt equilibria and how they behave during magma storage and decompression. These processes have a direct link on the type of volcanic activity that is taking place at Stromboli. However, our effort was to reconcile the large amount of data collected on this volcano with a plausible picture that explains how this volcano works. The first part of this review paper was concentrated in revisiting mineral phase stabilities in Stromboli basalt and how these, together with volatiles, may affect magma

767 compressibility during progressive decompression. In this perspective, one of the open issue we
768 attempted to unravel is the effective shape and extension of Stromboli magma chamber. In general,
769 the geometry and dynamics of magma chambers are still debated issues (e.g., Bonafede *et al.*, 1986;
770 Dragoni & Magnanesi, 1989; Jellinek & De Paolo, 2003). Unfortunately, these authors essentially
771 model magma chamber as spherical objects. In a recent contribution Zellmer & Annen (2008)
772 discussed a full variety of plumbing systems, and attempted to correlate their geometry with magma
773 transfer rates and magmatic differentiation processes. For instance, Stromboli is classified within
774 the field of relatively small reservoirs found within extensional (or transtensional) settings, where
775 the magma is stored for 10^3 years at the most. However, in a recent paper Mastin *et al.* (2008)
776 suggested a possible shape for Mount Saint Helen magma chamber that may be regarded as a
777 prolate ellipsoid. Moreover, Gudmudsson (2006) discussed the possible shapes of magma chambers
778 in relation to the structural setting of the region and indicates a prolate ellipsoid as a recurrent
779 shape. In our specific case we are dealing with a rather unique case where seismic data indicate that
780 the major structure underneath Stromboli is essentially a normal fault (the Stromboli-Panarea
781 alignment) with a minor right-lateral strike-slip component SW of Panarea (e.g., Caccamo *et al.*,
782 1996). According to Acocella *et al.* (2009) in the Stromboli area stress distribution approach pure
783 extensional regimes, being consistent with the earlier works of Tibaldi (2001; 2004) and Tibaldi *et*
784 *al.* (2003). Following Shaw (1980) and assuming that stress regimes are proportional to the
785 geometry of the reservoir (whose vertical extension can inferred by fine thermobarometry), we may
786 infer stress distribution and give more reliable estimates than those proposed earlier by Cigolini et
787 al. (2008) for the Stromboli magma chamber volume. Another open issue is how the system
788 pressurizes and what factors are involved in the development of this process. Allard et al. (2008)
789 have shown that the eruption rate during mild and persistent Strombolian activity is at most 0.02
790 m^3/sec, whereas input flow rates at depth may be as high as 0.3-0.6 m^3/sec. This mechanism will
791 progressively pressurize the "open" plumbing system until a critical threshold is reached and a
792 major eruptive cycle begins. In this context strain rates at the chamber walls seems to be a critical

793 factor that need to be investigated in details and could be one of the goals for future research
794 advancements.

795 In conclusion, current results can be summarised as follows:

796 i. The role of volatiles has been shown to be critical for identifying the equilibrium
797 conditions of Stromboli magma during magma storage and decompression.

798 ii. Thermobarometric estimates indicate that Stromboli primitive hydrous basaltic melts
799 (preserved as melt inclusions in olivine with 2-3.7 wt% H_2O) are in equilibrium with
800 forsteritic olivine and diopside at pressures of 200-340 MPa pressure and temperatures of
801 1150-1200°C for $X^{m}_{CO_2}$ comprised between 0.6 and 0.76 (which is quite similar to the
802 magmatic gas composition sampled at the crater rim). The higher pressure regimes are
803 representative of the base of the chamber, where the ferromagnesian phases may
804 crystallise and cumulate. A particular case is given by Ca-rich or ultracalcic melts that are
805 regarded as a result of decompression along a steep adiabatic and/or isothermal curve.
806 During this process the magma will crosscut the stability field of diopside and enter the
807 liquidus field. The earlier crystallized diopside is destabilized and will react with the melt
808 leading to the formation of *ultracalcic melts*. Pichavant et al. (2009) ealier discussed this
809 possibility and we hereby explain how this process is occurring and quantify the P-T
810 regimes associated with this dynamics.

811 iii. Ejected golden pumices (with 2-3 wt% H2O), are in equilibrium with Ca-pyroxene,
812 forsteritic olivine and anorthitic plagioclase at 150–220 MPa and temperatures
813 approaching 1120-1150°C. These materials likely represent the middle and main part of
814 the chamber.

815 iv. Evolved melt inclusions in Fe-richer olivine (ca. Fo_{70}) of the scorias show average
816 equilibration pressures of 78 (± 20) MPa, and temperatures 1138 (± 14)°C, being

indicative of crystallisation within the conduit or its root-zone that reaches the upper part of the chamber.

v. The lower part of the chamber is located at 11-13 km below the summit whereas the upper part of the chamber reaches 4.5-5 km below the summit itself;

vi. the magma chamber is substantially zoned and the undegassed magma is stored below the latter depth (and may be ejected as pumice during paroxysmal explosions and, more rarely, major explosions);

vii. during its storage, within the upper part of the chamber and within the dike feeding the summit craters, the magma undergoes progressive degassing, cooling and crystallisation. These processes are involved in the genesis of lavas and scorias (that represent the degassed magma reaching the surface).

viii. The Stromboli plumbing system consists of an ellipsoidal magma chamber of 1-2 km^3 in volume, likely a prolate ellipsoid whose upper part is connected with the feeder dike.

ix. during major eruptions associated with lava effusions the dike feeding the summit vents is substantially rejuvenated and the upper part of the chamber is progressively replenished by the undegassed magma. During the 2007 eruption, the original magmastatic equilibrium was restored in about 230 days from the beginning of the effusive activity (as inferred by our analysis on SO_2-derived magma fluxes).

Acknowledgements

The research was funded by the University of Torino - Fondazione Compagnia di San Paolo. Additional funds were provided by MIUR and made available through the Cooperative Project among the Departments of Earth Sciences of the University of Torino and the University of Firenze (in the framework of the Devnet Project, funded by the Dipartimento della Protezione Civile, DPC). We are indebted to M. Ripepe and M. Pichavant for the stimulating discussions. We also thank Sébastien Jego and an anonymous reviewer for revising an earlier draft of the paper. Special

acknowledgements to INGV-Catania for making the SO_2 data available on the web. Additional funds for the improving our computing hardware were provided by Fondazione Cassa di Risparmio di Torino..

APPENDIX

We hereby report Table A1, A2 and A3 that summarizes the results of thermodynamic calculations regarding reactions (1) (2) and (3) that enabled us to construct Fig. 6.

Table A1, Table A2, Table A3

In Table A4 we summarize the list of symbols used in the equations discussed in the text.

Table A4

In Table A5 we report step-by-step calculations for the isothermal decompression of a primitive Stromboli basalt (cf., Fig. 9).

Table A5

References

Acocella, V., Neri, M. & Walter, T.H. 2009. Structural features of Panarea volcano in the frame of the Aeolian Arc (Italy): Implications for the 2002–2003 unrest. *Journal of Geodynamics*, **47**, 288–292.

Aiuppa, A., Inguaggiato, S., McGonigle, A.J.S., O'Dwyer, M., Oppenheimer, C., Padgett, M.J., Rouwet, D. & Valenza, M. 2005. H_2S fluxes from Mt. Etna, Stromboli, and Vulcano (Italy) and implications for the sulphur budget at volcanoes. *Geochimica et Cosmochimica Acta*, **69(7)**, 1861-1871.

Aiuppa, A., Federico, C., Giudice, G., Giuffrida, G., Guida, R., Gurrieri, S., Liuzzo, M., Moretti, R. & Papale, P. 2009. The 2007 eruption of Stromboli volcano: Insights from real-time measurement of the volcanic gas plume CO_2/SO_2 ratio. *Journal of Volcanology and Geothermal Research*, **182(3-4)**, 221-230.

Aiuppa, A., Bertagnini, A., Métrich, N., Moretti, R., Di Muro, A., Liuzzo, M. & Tamburello, G. 2010a. A model of degassing for Stromboli volcano. *Earth and Planetary Science Letters*, **295(1-2)**, 195-204.

Aiuppa, A., Burton, M., Caltabiano, T., Giudice, G., Guerrieri, S., Liuzzo, M., Mur, F. & Salerno, G. 2010b. Unusually large magmatic CO2 gas emissions prior to a basaltic paroxysm. *Geophysical Research Letters*, **37(17)**, L17303.

Aiuppa, A., Burton, M., Allard, P., Caltabiano, T., Giudice, G., Gurrieri, S., Liuzzo, M. & Salerno, G. 2011. First observational evidence for the CO2-driven origin of Stromboli's major explosions. *Solid Earth*, **2(2)**, 135-142.

Aki, K. & Ferrazzini, V. (2001). Comparison of Mount Etna, Kilauea, and Piton de la Fournaise by a quantitative modeling of their eruption histories (Review). *Journal of Geophysical Research B: Solid Earth*, **106B3**, 4091-4102.

Allard, P., Aiuppa, A., Burton, M., Caltabiano, T., Federico, C., Salerno, G. & La Spina, A. 2008. Crater Gas Emissions and the Magma Feeding System of Stromboli Volcano. *In*: Calvari, S., Inguaggiato, S., Ripepe, M. & Rosi, M. (eds.) *The Stromboli volcano: an integrated study of the 2002–2003 eruption*. AGU, Geophysical Monograph Series, Washington D.C., **182**, 65–80.

Arrighi, S., Rosi, M., Tanguy, J. & Courtillot, V. 2004. Recent eruptive history of Stromboli (Aeolian Islands, Italy) determined from high-accuracy archeomagnetic dating. *Geophysical Research Letters*, **31**, doi:10.1029/2004GL020627.

Barberi, F., Rosi, M. & Sodi, A., 1993. Volcanic hazard assessment at Stromboli based on review of historical data. *Acta Vulcanologica*, **3**, 173-187.

Beattie P. 1993. Olivine-melt and orthopyroxene-melt equilibria. *Contribution to Mineralogy and Petrology*, **115**:103-111.

Berman, R.G. 1988. Internally consistent thermodynamic data for stoichiometric minerals in the system Na_2O-K_2O-CaO-MgO-FeO-Fe_2O_3-Al_2O_3-SiO_2-TiO_2-H_2O-CO_2. *Journal of Petrology*, **29**, 445-522.

Bertagnini, A., Métrich, N., Landi, P. & Rosi, M. 2003. Stromboli volcano (Aeolian Archipelago, Italy): An open window on the deep-feeding system of a steady state basaltic volcano. *Journal of Geophysical Research B: Solid Earth*, **108(7)**, ECV 4-1–4-15.

Bertagnini, A., Métrich, N., Francalanci, L., Landi, P., Tommasini, S. & Conticelli, S. 2008. Volcanology and magma geochemistry of the present-day activity: constraints on the feeding system. *In*: Calvari, S., Inguaggiato, S., Ripepe, M. & Rosi, M. (eds.) *The Stromboli volcano: an integrated study of the 2002–2003 eruption*. AGU, Geophysical Monograph Series, Washington D.C., **182**, 19–38.

925 Bertagnini, A., Di Roberto, A. & Pompilio, M. 2011. Paroxysmal activity at Stromboli: Lessons
926 from the past. *Bulletin of Volcanology*, **73(9)**, 1229-1243.
927
928 Bonaccorso, A., Gambino, S., Guglielmino, F., Mattia, M., Puglisi, G. & Boschi, E. 2008.
929 Stromboli 2007 eruption: Deflation modeling to infer shallow-intermediate plumbing system.
930 *Geophysical Research Letters*, **35(6)**, L06311.
931
932 Bonafede, M., Dragoni, M. & Quareni, F., 1986. Displacement and stress fields produced by a
933 centre of dilatation and by a pressure source in a viscoelastic half-space: application to the study of
934 ground deformation and seismic activity at Campi Flegrei, Italy. *Geophysical Journal of the Royal*
935 *Astronomical Society*, **87**, 455–485.
936
937 Burton, M., Allard, P., Mure, F. & La Spina, A. 2007. Magmatic gas composition reveals the source
938 depth of slug-driven strombolian explosive activity. *Science*, **317(5835)**, 227-230.
939
940 Burton, M.R., Caltabiano, T., Murè, F., Salerno, G. & Randazzo, D. 2009. SO_2 flux from Stromboli
941 during the 2007 eruption: Results from the FLAME network and traverse measurements. *Journal of*
942 *Volcanology and Geothermal Research*, **182(3-4)**, 214-220.
943
944 Caccamo, D., Neri, G., Sarao, A. & Wiss, M. 1996. Estimates of stress directions by inversion of
945 earthquake fault-plane solutions in Sicily. *Geophysical Journal International*, **125/3**, 857-858.
946
947 Calvari, S., Spampinato, L., Lodato, L., Harris, A.J.L., Patrick, M., Dehn, J., Burton, M.R. &
948 Andronico, D. 2005. Chronology and complex volcanic processes during the 2002–2003 flank
949 eruption at Stromboli volcano (Italy) reconstructed from direct observations and surveys with a

handheld thermal camera. *Journal of Geophysical Research*, **110**, B02201, doi:10.1029/2004JB003129.

Calvari, S., Lodato, L., Steffke, A., Cristaldi, A., Harris, A.J.L., Spampinato, L. & Boschi, E. 2010. The 2007 stromboli eruption: Event chronology and effusion rates using thermal infrared data. *Journal of Geophysical Research B: Solid Earth*, **115(4)**, B04201.

Calvari, S., Spampinato, L., Bonaccorso, A., Oppenheimer, C., Rivalta, E. & Boschi, E. 2011. Lava effusion-A slow fuse for paroxysms at Stromboli volcano? *Earth and Planetary Science Letters*, **301(1-2)**, 317-323.

Carapezza, M.L. & Federico, C. 2000. The contribution of fluid geochemistry to the volcano monitoring of Stromboli. *Journal of Volcanology and Geothermal Research*, **95(1-4)**, 227-245.

Carapezza, M.L., Ricci, T., Ranaldi, M. & Tarchini, L. 2009. Active degassing structures of Stromboli and variations in diffuse CO2 output related to the volcanic activity. *Journal of Volcanology and Geothermal Research*, **182(3-4)**, 231-245.

Chiodini, G. & Cioni, R. 1989. Gas barometry for hydrothermal systems and its application to some Italian geothermal areas. *Applied Geochemistry*, **4**, 465-472.

Chiodini, G. & Marini, L. 1998. Hydrothermal gas equilibria: The H_2O-H_2-CO_2-CO-CH_4 system. *Geochimica et Cosmochimica Acta*, **62(15)**, 2673-2687, doi:10.1016/S0016-7037(98)00181-1.

Cigolini, C., Laiolo, M. & Bertolino, S. 2008. Probing Stromboli volcano from the mantle to paroxysmal eruptions. *In*: Zellmer, G. & Hammer, J. (eds.) *Dynamics of Crustal Magma Transfer,*

976 *Storage, and Differentiation – integrating geochemical and geophysical constraints*. Geological
977 Society, London, Special Publication, **304**, 33-70.
978
979 Cigolini, C., Poggi, P., Ripepe, M., Laiolo, M., Ciamberlini, C., Delle Donne, D., Ulivieri, G.,
980 Coppola, D., Lacanna, G., Marchetti, E., Piscopo, D. & Genco, R. 2009. Radon surveys and real-
981 time monitoring at Stromboli volcano: influence of soil temperature, atmospheric pressure and tidal
982 forces on 222Rn degassing. *Journal of Volcanology and Geothermal Research*, **184(3-4)**, 381-388.
983
984 Cigolini, C., Laiolo, M., Ulivieri, G., Coppola, D. & Ripepe, M. 2013. Radon mapping, automatic
985 measurements and extremely high ^{222}Rn emissions during the 2002–2007 eruptive scenarios at
986 Stromboli volcano. *Journal of Volcanology and Geothermal Research*, **264**, 49-65.
987
988 Conte, A.M., Perinelli, C. & Trigila, R. 2006. Cooling kinetics experiments on Stromboli lavas of
989 different serial affinity giving variable crystal morphologies and phases composition. *Journal of*
990 *Volcanology and Geothermal Research*, **155**, 179-200.
991
992 Coppola, D., Piscopo, D., Laiolo, M., Cigolini, C., Delle Donne, D. & Ripepe, M. 2012. Radiative
993 heat power at Stromboli volcano during 2000-2011: twelve years of MODIS observations. *Journal*
994 *of Volcanology and Geothermal Research*, **215–216**, 48-60.
995
996 Corazzato, C., Francalanci, L., Menna, M., Petrone, C.M., Renzulli, A., Tibaldi, A. & Vezzoli, L.
997 2008. What controls sheet intrusion in volcanoes? Structure and petrology of the Stromboli sheet
998 complex, Italy. *Journal of Volcanology and Geothermal Research*, **173**, 26–54.
999

1000 D'Auria, L., Giudicepietro, F., Martini, M., & Orazi, M. 2006. *The April–May 2006 volcano-*
1001 *tectonic events at Stromboli volcano (Southern Italy) and their relation with the magmatic system*.
1002 Earth-Prints open archives, http://www.earth-prints.org/handle/2122/1506.
1003
1004 Danyushevsky, L.V., Leslie, R.A.J., Crawford, A.J. & Durance, P. 2004. Melt inclusions in
1005 primitive olivine phenocrysts: The role of localized reaction processes in the origin of anomalous
1006 compositions. *Journal of Petrology*, **45**, 2531-2553.
1007
1008 De Astis, G., Ventura, G. & Vilardo, G. 2003. Geodymanic significance of the Aeolian volcanism
1009 (Southern Tyrrhenian Sea, Italy) in light of structural, seismological and geochemical data.
1010 *Tectonics*, **22**, doi:10.1029/2003TC001506,2003.
1011
1012 Di Carlo, I., Pichavant, M., Rotolo, S.G. & Scaillet, B. 2006. Experimental crystallization of a High
1013 K-arc basalt: the golden pumice, Stromboli Volcano. *Journal of Petrology*, **47**, 1317-1343.
1014
1015 Dixon, J.E. 1997. Degassing of alkalic basalts. *American Mineralogist*, **82(3-4)**, 368-378.
1016
1017 Dixon, J.E. & Stolper, E.M. 1995. An experimental study of water and carbon dioxide solubilities
1018 in mid-ocean ridge basaltic liquids. Part II: Applications to degassing. *Journal of Petrology*, **36**,
1019 1633–1646.
1020
1021 Dragoni M. & Magnanensi, C. 1989. Displacement and stress produced by a pressurized, spherical
1022 magma chamber, surrounded by a viscoelastic shell. *Physics of the Earth and Planetary Interiors*,
1023 **56**, 316-328.
1024

1025 Finizola, A., Sortino F., Lénat, J.F., Aubert, M., Ripepe M. & Valenza, M., 2003. The summit
1026 hydrothermal system of Stromboli. New insights from self-potential, temperature, CO2 and
1027 fumarolic fluid measurements, with structural and monitoring implications. *Bulletin of Volcanology*
1028 **65**, 486–504. doi:10.1007/s00445-003-0276-z.
1029
1030 Fornaciai, A., Landi, P. & Armienti, P. 2009. Dissolution/crystallization kinetics recorded in the
1031 2002-2003 lavas of Stromboli (Italy). *Bulletin of Volcanology*, **71(6)**, 631-641.
1032
1033 Francalanci, L., Manetti, P., Peccerillo, A. & Keller, J. 1993. Magmatological evolution of the
1034 Stromboli volcano (Aeolian Arc, Italy): inferences from major and trace element and Sr isotopic
1035 composition of lavas and pyroclastic rocks. *Acta Vulcanologica*, **3**, 127-151.
1036
1037 Francalanci, L., Tommasini, S., Conticelli, S. & Davies, G.R. 1999. Sr isotope evidence for short
1038 magma residence time for the 20th century activity at Stromboli volcano, Italy. *Earth and Planetary*
1039 *Science Letters*, **167(1-2)**, 61-69.
1040
1041 Francalanci, L., Tommasini, S. & Conticelli, S. 2004. The volcanic activity of Stromboli in the
1042 1906-1998 AD period: Mineralogical, geochemical and isotope data relevant to the understanding
1043 of the plumbing system. *Journal of Volcanology and Geothermal Research*, **131(1-2)**, 179-211.
1044
1045 Gasparik, T. 1984. Two pyroxene thermobarometry with new experimental data in the CaO-MgO-
1046 Al_2O_3-SiO_2. *Contribution to Mineralogy and Petrology*, **87**, 87-97.
1047
1048 Gasparik., T. 1990. A thermodynamic model for the enstatite-diopside join. *American Mineralogist*,
1049 **75**, 1080-1091.
1050

1051 Ghiorso, M.S. & Sack, R.O. 1995. Chemical mass transfer in magmatic processes: IV A revised and
1052 internally consistent thermodynamic model for the interpolation and extrapolation of liquid-solid
1053 equilibria in magmatic systems at elevated temperature and pressures. *Contribution to Mineralogy*
1054 *and Petrology*, **119**, 197-212.
1055
1056 Gillot, P.Y. & Keller, J. 1993. Radiochronological dating of Stromboli. *Acta Vulcanologica*, **3**, 69-
1057 77.
1058
1059 Gudmundsson, A. 2006. How local stresses control magma-chamber ruptures, dyke injections, and
1060 eruptions in composite volcanoes. *Earth Science Reviews*, **79(1-2)**, 1-31.
1061
1062 Gvirtzman, Z. & Nur, A. 2001. Residual topography, lithospheric structure and sunken slabs in the
1063 central Mediterranean. *Earth and Planetary Science Letters*, **187**, 117-130.
1064
1065 Harris, A.J.L., Murray, J.B., Aries, S.E., Davies, M.A., Flynn, L.P., Wooster, M.J., Wright, R. &
1066 Rothery, D.A. 2000. Effusion rate trends at Etna and Krafla and their implications for eruptive
1067 mechanisms. *Journal of Volcanology and Geothermal Research*, **102(3-4)**, 237-270.
1068
1069 Helz, R.T. & Thornber, C.R. 1987. Geothermometry of Kilauea Iki lava lake, Hawaii. *Bulletin of*
1070 *Volcanology*, **49**, 651-668.
1071
1072 Holloway, J.R. 1977. Fugacity and activity of molecular species in supercritical fluids. *In*: Faser D.
1073 (eds.) *Thermodynamics in Geology*, 161–181.
1074

1075 Hornig-Kjarsgaard, I., Keller, J., Koberski, U., Stadbauer, E., Francalanci, L. & Lenhart, R. 1993.
1076 Geology, stratigraphy and volcanological evolution of the island of Stromboli, Aeolian arc, Italy.
1077 *Acta Vulcanologica* , **3**, 21-68.
1078
1079 Hübner, J.S. & Sato, M. 1970. The oxygen fugacity-temperature relationships of manganese oxide
1080 and nickel oxide buffers. *American Mineralogist*, **55**, 934-952.
1081
1082 Huppert, H.E. & Woods, A.W. 2002. The role of volatiles in magma chamber dynamics. *Nature*,
1083 **420(6915)**, 493-5.
1084
1085 Jellinek, A.M. & DePaolo, D.J. 2003. A model for the origin of large silicic magma chambers:
1086 precursors of caldera-forming eruptions. *Bulletin of Volcanology*, **65**, 363–381,
1087 doi:10.1007/s00445-003-0277-y.
1088
1089 Kamenetsky, V.S., Eggins, S.M., Crawford, A.J., Green, D.H., Gasparon, M. & Falloon, T.J. 1998.
1090 Calcic melt inclusions in primitive olivine at 43°N MAR: evidence for melt–rock reaction/melting
1091 involving clinopyroxene-rich lithologies during MORB generation. *Earth and Planetary Science*
1092 *Letters*, **160**, 115–132.
1093
1094 Keller, J., Hornig-Kjarsgaard, I., Koberski, U., Stadlbauer, E. & Lenhard, R. 1993. Geological Map
1095 of Stromboli 1:10000. *Acta Vulcanologica*, **3**.
1096
1097 Kress, V.C. & Carmichael, I.S.E. 1991. The compressibility of silicate liquids containing Fe_2O_3 and
1098 the effect of composition, temperature, oxygen fugacity and pressure on their redox states.
1099 *Contribution to Mineralogy and Petrology*, **108(1-2)**, 82-92.
1100

1101 Kushiro, I. 1979. Fractional crystallization of basaltic magma. *In*: Yoder H.S. (eds.), *The Evolution*
1102 *of Igneous Rocks*. Princeton University Press, Princeton, 171-199.
1103
1104 Laiolo, M. & Cigolini, C. 2006. Mafic and Ultramafic xenoliths of San Bartolo lava field: new
1105 insight on the ascent and storage of Strombolian magmas. *Bulletin of Volcanology*, **68**, 653-670.
1106
1107 Laiolo, M., Cigolini, C., Coppola, D. & Piscopo, D. 2012. Developments in real-time radon
1108 monitoring at Stromboli volcano. *Journal of Environmental Radioactivity*, **105**, 21–29.
1109
1110 Landi, P., Métrich, N., Bertagnini, A. & Rosi, M. 2004. Dynamics of magma mixing and degassing
1111 recorded in plagioclase at Stromboli (Aeolian Archipelago, Italy). *Contributions to Mineralogy and*
1112 *Petrology*, **147(2)**, 213-227.
1113
1114 Landi, P., Francalanci, L., Pompilio, M., Rosi, M., Corsaro, R.A., Petrone, C.M., Nardini, I. &
1115 Miraglia, L. 2006. The December 2002-July 2003 effusive event at Stromboli volcano, Italy:
1116 Insights into the shallow plumbing system by petrochemical studies. *Journal of Volcanology and*
1117 *Geothermal Research*, **155(3-4)**, 263-284.
1118
1119 Landi, P., Corsaro, R.A., Francalanci, L., Civetta, L., Miraglia, L., Pompilio, M. & Tesoro, R. 2009.
1120 Magma dynamics during the 2007 Stromboli eruption (Aeolian Islands, Italy): mineralogical,
1121 geochemical and isotopic data. *Journal of Volcanology and Geothermal Research*, **182(3-4)**, 255–
1122 268.
1123
1124 Lange, R.A. & Carmichael, I.S.E. 1990. Thermodynamic properties of silicate liquids with
1125 emphasis on density, thermal expansion and compressibility. *In*: Nicholls, J. & Russell, J.K. (eds.)

Modern methods of igneous petrology: understanding magmatic processes. Reviews in Mineralogy and Geochemistry, **24**, 25-59.

La Spina, A., Burton, M.R., Harig, R., Mure, F., Rusch, P., Jordan, M. & Caltabiano, T. 2013. New insights into volcanic processes at Stromboli from Cerberus, a remote-controlled open-path FTIR scanner system. *Journal of Volcanology and Geothermal Research*, **249**, 66-76.

Marsella, M., Proietti, C., Sonnessa, A., Coltelli, M., Tommasi, P. & Bernardo, E. 2009. The evolution of the Sciara del Fuoco subaerial slope during the 2007 Stromboli eruption: Relation between deformation processes and effusive activity. *Journal of Volcanology and Geothermal Research*, **182(3-4)**, 201-213.

Marsella, M., Baldi, P., Coltelli, M. & Fabris, M. 2012. The morphological evolution of the Sciara del Fuoco since 1868: Reconstructing the effusive activity at Stromboli volcano. *Bulletin of Volcanology*, **74(1)**, 231-248.

Martini, M., Buccianti, A., Capaccioni, B., Giannini, L. & Prati, F. 1996. Fumarole gas analysis (Stromboli). *Acta Vulcanoogica*, **6**, 53-54.

Mastin, L.G. & Ghiorso, M.S. 2000. *A Numerical Program for Steady-State Flow of Magma-Gas Mixtures Through Vertical Eruptive Conduits*. U.S. Geological Survey Open-File Report, **00209**.

Mastin, L.G., Roeloffs, E., Beeler, N.M. & Quick, J.E. 2008. *Constraints on the size, overpressure, and volatile content of the Mount St. Helens magma system from geodetic and dome-growth measurements during the 2004-2006 eruption*. US Geological Survey Professional Paper, **1750**, 461-492.

Métrich, N. & Clocchiatti, R. 1996. Sulphur abundance and its speciation in oxidized alkaline melts. *Geochimica et Cosmochimica Acta*, **60(21)**, 4151-4160.

Métrich, N., Bertagnini, A., Landi, P. & Rosi, M. 2001. Crystallization driven by decompression and water loss at Stromboli volcano (Aeolian Islands, Italy). *Journal of Petrology*, 42(8), 1471-1490.

Métrich, N.A., Bertagnini, A., Landi, P. & Rosi, M. 2005. Triggering mechanism at the origin of paroxysm at Stromboli (Aeolian Archipelago, Italy): The 5 April 2003 eruption. *Geophysical Research Letters*, **32**, L10305.

Métrich, N.A., Bertagnini, A. & Di Muro, A. 2010. Conditions of Magma Storage, Degassing and Ascent at Stromboli: New Insights into the Volcano Plumbing System with Inferences on the Eruptive Dynamics. *Journal of Petrology*, **51**, 603-626.

Métrich, N., Allard, P., Bertagnini, A. & Di Muro, A. 2011. Comment on 'Conduit convection, magma mixing, and melt inclusion trends at persistent degassing volcanoes' by Fred Witham, published in Earth Planetary Science Letters (2011) 301, 345-352. *Earth and Planetary Science Letters*, **306 (3-4)**, 306-308, doi: 10.1016/j.epsl.2011.04.012.

Mysen, B. & Boettcher, A.L. 1975a. Melting of a hydrous mantle: I. Phase relations of natural peridotite at high pressures and temperatures with controlled activities of water, carbon dioxide, and hydrogen. *Journal of Petrology*, **16(1)**, 520-548.

1177 Mysen, B. & Boettcher, A.L. 1975b. Melting of a hydrous mantle: II. Geochemistry of crystals and
1178 liquids formed by anatexis of mantle peridotite at high pressures and high temperatures as a
1179 function of controlled activities of water, hydrogen, and carbon dioxide. *Journal of Petrology*,
1180 **16(1)**, 549-593.
1181
1182 Neri, M. & Lanzafame, G., 2009. Structural features of the 2007 Stromboli eruption. *Journal of*
1183 *Volcanology and Geothermal Research*, **182(3-4)**, 137–144.
1184
1185 Newhall, C.G. & Self, S. 1982. The volcanic explosivity index (VEI): An estimate of explosive
1186 magnitude for historical volcanism. *Journal of Geophysical Research*, **87**, 1231-1238.
1187
1188 Newman, S. & Lowenstern, J.B. 2002. VOLATILECALC: A silicate melt-H_2O-CO_2 solution model
1189 written in Visual Basic for excel. *Computers and Geosciences*, **28(5)**, 597-604, doi:10.1016/S0098-
1190 3004(01)00081-4.
1191
1192 Newton, R.C., Ciarlo, T.V. & Kleppa, O.J. 1980. Thermochemistry of the high structural state of
1193 plagioclase. *Geochimica et Cosmochimica Acta*, **75**, 369-376.
1194
1195 Palma, J.L., Blake, S. & Calder, E.S. 2011. Constraints on the rates of degassing and convection in
1196 basaltic open-vent volcanoes. *Geochemistry, geophysics and geosystems*, **12**, Q11006.
1197 doi:10.1029/2011GC003715.
1198
1199 Papale, P., Moretti, R. & Barbato, D. 2006. The compositional dependence of the saturation surface
1200 of H_2O+CO_2 fluids in silicate melts. *Chemical Geology*, **229**, 78-95.
1201

Pearce, T. H. & Stanley, C.R. 1991. The validity of Pearce Element Ratio analysis in petrology: An example from the Uwekahuna Laccolith, Hawaii. *Contributions to Mineralogy and Petrology*, **108**, 212-218.

Peccerillo, A. 2001. Geochemical similarities between the Vesuvius, Phlegraean Fields and Stromboli Volcanoes: petrogenetic, geodynamic and volcanological implications. *Mineralogy and Petrology*, **73**, 93-105.

Peccerillo, A. & Taylor, S.R. 1976. Geochemistry of Eocene Calc-Alkaline volcanic rocks from Kastamorun area, Northern Turkey. *Contribution to Mineralogy and Petrology*, **58**, 63-81.

Pichavant, M., Di Carlo, I., Le Gac, Y., Rotolo, S.G. & Scaillet, B. 2009. Experimental Constraints on the Deep Magma Feeding System at Stromboli Volcano, Italy. *Journal of Petrology*, **50(4)**, 601-624.

Pompilio, M., Bertagnini, A. & Métrich, N. 2012. Geochemical heterogeneities and dynamics of magmas within the plumbing system of a persistently active volcano: Evidence from Stromboli. *Bulletin of Volcanology*, **74(4)**, 881-894.

Pontevivo, A. & Panza, G.F., 2006. The Lithosphere-Asthenosphere System in the Calabrian Arc and Surrounding Seas – Southern Italy. *Pure and Applied Geophysics*, **163**, 1617–1659.

Putirka, K., Ryerson, F.J. & Mikaelian, H. 2003. New igneous thermobarometers for mafic and evolved lava compositions, based on clinopyroxene + liquid equilibria. *American Mineralogist*, **88**, 1542-1554.

1228 Putirka, K.D. 2008. Thermometers and barometers for Volcanic Systems. *In*: Putirka, K.D. &
1229 Tepley III, F.J. (eds.) *Minerals, inclusions and volcanic processes*. Reviews in Mineralogy &
1230 Geochemistry, **69**, 61-120.
1231
1232 Richet, P., Bottinga, Y., Denielou, L., Petitet, J.P. & Tequi, C. 1982. Thermodynamic properties of
1233 quartz, crystobalite and amorphous SiO_2: drop calorimetry measurements between 1000 and 1800
1234 °K and a review from 0 to 2000°K. *Geochimica et Cosmochimica Acta*, **46**, 2639-2658.
1235
1236 Ripepe, M., Marchetti, E., Ulivieri, G., Harris, A.J., Dehn, J., Burton, M., Caltabiano, T. & Salerno,
1237 G. 2005. Effusive to explosive transition during the 2003 eruption of Stromboli volcano. *Geology*,
1238 **33(5)**, 341-344.
1239
1240 Rizzo, A., Grassa, F., Inguaggiato, S., Liotta, M., Longo, M., Madonia, P., Brusca, L., Capasso, G.,
1241 Moricia, S., Rouwet, D. & Vita, F. 2009. Geochemical evaluation of observed changes in volcanic
1242 activity during the 2007 eruption at Stromboli (Italy). *Journal of Volcanology and Geothermal*
1243 *Research*, **182(3-4)**, 246-254.
1244
1245 Robie, R.A., Hemingway, B.S. & Fisher, J.R. 1979. *Thermodynamic properties of minerals and*
1246 *related substances at 218.15 K and 1 Bar (105 Pascals), Pressure and Higher Temperatures*. USGS
1247 Bullettin, **1452**.
1248
1249 Roeder, P.L. & Emslie, R.F. 1970. Olivine-liquid equilibrium. *Contributions to Mineralogy and*
1250 *Petrology*, **29**, 275–289.
1251
1252 Russell, J.K. & Nicholls, J. 1988. Analysis of petrologic hypotheses with Pearce element ratio.
1253 *Contributions to Mineralogy and Petrology*, **99**, 25-35.

Sack, R.O. & Ghiorso, M.S. 1989. Importance of considerations of mixing properties in establishing an internally consistent thermodynamic database: thermochemistry of minerals in the system Mg_2SiO_4-Fe_2SiO_4-SiO_2. *Contributions to Mineralogy and Petrology*, **102**, 41-68.

Schiavi, F., Kobayashi, K., Nakamura, E., Tiepolo, M. & Vannucci, R. 2012. Trace element and Pb-B-Li isotope systematics of olivine-hosted melt inclusions: Insights into source metasomatism beneath Stromboli (southern Italy). *Contributions to Mineralogy and Petrology*, **163(6)**, 1011-1031.

Shaw, H.R. 1980. The fracture mechanism of magma transport from the mantle to the surface. *In*: Hargaves, R.B. (eds.) *Physics of Magmatic Processes*. Princeton University Press, 201-264.

Silver, L.A. & Stolper, E.M. 1985. A thermodynamic model for hydrous silicate melts. *Journal of Geology*, **93**, 161-178.

Sisson, T.W. & Grove, T.L. 1993. Temperatures and H_2O contents of low-MgO high-alumina basalts. *Contributions to Mineralogy and Petrology*, **113**, 167-184.

Speranza, F., Pompilio, M., Caracciolo, F.D. & Sagnotti, L. 2008. Holocene eruptive history of the Stromboli volcano: Constraints from paleomagnetic dating. *Journal of Geophysical Research B: Solid Earth*, **113(9)**, B09101.

Stasiuk, M.V., Jaupart, C. & Sparks, R.S.J. 1993. On the variations of flow rate in non-explosive lava eruptions. *Earth and Planetary Science Letters*, **134**, 505–516.

1279 Stevenson, D.S. & Blake, S. 1998. Modelling the dynamics and thermodynamics of volcanic
1280 degassing. *Bulletin of Volcanology*, **60**, 307-317.
1281
1282 Tazieff, H. & Tonani, F. 1963. Fluctuations rapides et importantes de la phase gazeuse éruptive.
1283 *Comptes Rendus de l'Académie des Sciences,* Paris, **257**, 3985-3987.
1284
1285 Tamburello, G., Aiuppa, A., Kantzas, E.P., McGonigle, A.J.S. & Ripepe, M. 2012. Passive vs.
1286 active degassing modes at an open-vent volcano (Stromboli, Italy). Earth and Planetary Science
1287 Letters, 359-360, 106-116.
1288
1289 Tibaldi, A. 2001. Multiple sector collapses at Stromboli volcano, Italy: How they work. *Bulletin of*
1290 *Volcanology*, **63(2-3)**, 112-125.
1291
1292 Tibaldi, A. 2004. Major changes in volcano behaviour after a sector collapse: insights from
1293 Stromboli, Italy. *Terra Nova*, **16**, 2-8.
1294
1295 Tibaldi, A., Corazzato, C., Apuani, T., Cancelli, A. 2003. Deformation at Stromboli volcano (Italy)
1296 revealed by rock mechanics and structural geology. *Tectonophysics*, **361(3-4)**, 187-204.
1297
1298 Tibaldi, A., Corazzato, C., Marani, M. & Gamberi, F. 2009. Subaerial-submarine evidence of
1299 structures feeding magma to Stromboli Volcano, Italy, and relations with edifice flank failure and
1300 creep. *Tectonophysics*, **469**, 112–136.
1301
1302 Ventura, G., Vilardo, G., Milano, G. & Pino, N.A. 1999. Relationships among crustal structure,
1303 volcanism and strike-slip tectonics in the Lipari-Vulcano volcanic complex. *Physics of the Earth*
1304 *and Planetary Interiors*, **116**, 31-52.

Ventura G. 2013. Kinematics of the Aeolian volcanism (Southern Tyrrhenian Sea) from geophysical and geological data. In: Lucchi, F., Peccerillo, A., Keller, J., Tranne, C. A. & Rossi, P. L. (eds) The Aeolian Islands Volcanoes. Geological Society, London, Memoirs, 37, 3–11. http://dx.doi.org/10.1144/M37.2.

Wadge, G. 1981, The variation of magma discharge during basaltic eruptions: *Journal of Volcanology and Geothermal Research*, **11**, 139–168.

Witham, F. 2011a. Conduit convection, magma mixing, and melt inclusion trends at persistently degassing volcanoes. *Earth and Planetary Science Letters*, **301(1-2)**, 345-352, doi: 10.1016/j.epsl.2010.11.017.

Witham, F. 2011b. Conduit convection, magma mixing, and melt inclusion trends at persistently degassing volcanoes: Reply to comment by Métrich et al. (2011). *Earth and Planetary Science Letters*, **306(3-4)**, 309-311.

Wyllie, P.J. 1979. Magmas and volatile components. *American Mineralogist*, **64**, 469-500.

Yoder, H.S. Jr. (1969). Calcalkalic andesites: experimental data bearing on the origin of their assumed characteristics. *In*: McBirney A.R. (eds.), *Proceeding of the Andesite Conference*. Oreg. Dep.Geol.Miner.Ind.Bull., **65**, 77-89.

Zellmer, G.F. & Annen, C. 2008. An introduction to magma dynamics. *In*: Zellemr, G. & Hammer, J. (eds.) *Dynamics of Crustal Magma Transfer, Storage, and Differentiation – integrating*

geochemical and geophysical constraints. Geological Society, London, Special Publication, **304**, 33-70.

Figure Captions

Fig. 1. Sketch of the Aeolian Islands with the major tectonic units of the region (modified after De Astis *et al*., 2003; Ventura et al., 2013). **(a)** Stromboli is located on the Stromboli-Panarea alignment, a normal fault associated with pure extensional regimes (Acocella *et al*., 2009). Insets show the crust-mantle structure along a WNW-ESE cross section (cf. Pontevivo & Panza, 2006; Corazzato *et al.,* 2008), and the summary of earthquake locations and magnitudes below the Aeolian arc. The earthquakes reported are included within a sector with 37°-40° latitude, and 12°-15° longitude, respectively (see text for details). LVZ: low velocity zone;
b) simplified geological map of Stromboli with major collapses and faults (modified after Hornig-Kjarsgaard *et al*., 1993; Tibaldi *et al*., 2009).

Fig. 2. Selected images of Stromboli volcano during and following the 2007 major eruption; **(a)** the 2007 lava field emplaced onto earlier lavas and debris of Sciara del Fuoco. Picture taken on August 3, 2007 during a helicopter survey; **(b)** view of the summit crater area where the typical strombolian activity was resumed on July 2, 2007. Summit vents are located on the N40°E graben-like fracture zone (red dashed line). Picture taken on August 3, 2007 during a helicopter survey.

Fig. 3. Microphotographs of the petrographic and textural features of Stromboli lavas, scorias and pumices erupted in 2002-2003; **a)** *scoria* erupted on February 16, 2007 with euhedral phenocrysts of plagioclase, and clinopyroxene on a glassy matrix. Vesicles are also present (white). Scorias are

interpreted as "conduit assemblages". Plane polarized light; **b)** microphotograph of lava erupted in March, 2007 during the last effusive event. Lava is phenocrysts-rich (around 40%) mainly represented by clinopyroxene and plagioclase, with the typical oscillatory zoning. Vesiculation is relatively high. Plane polarized light; **c)** Photomicrograph of a quenched *"golden pumice"* erupted during the paroxysmal explosion of March 15, 2007. Vesicularity is very high (~70%) with bubbles of variable size and low degree of cristallinity (<10%) with microliths of plagioclase, clinopyroxene and olivine (not visible at this scale). Plane polarized light.

Fig. 4. Low silica-moderate K_2O sector of the diagram of Peccerillo and Taylor (1976) with the plotting of the available data on the materials erupted at Stromboli; **a)** lavas and scorias, including matrix glasses. Grey fields refer to historical materials erupted from Stromboli volcano since 1906 (these data were summarized by Francalanci *et al.*, 2004; Pompilio *et al.*, 2012). The dark grey field show the glass composition of the 2002-2003 and 2007 erupted materials (data reported by Landi *et al.*, 2006; 2009) ; **b)** pumices erupted during paroxysmal and major explosions; melt inclusions are those reported by Métrich *et al.* (2001; 2005; 2010) Bertagnini *et al*. (2003). The grey field shows the bulk composition of the hystorical pumices reported by Pompilio *et al*. (2012).

Fig. 5. Pearce element ratio plots for Stromboli materials (including melt inclusions in olivines of the pumices); **a)** 2Ca+3Na/K versus Si/K diagram indicates fractionation of clinopyroxene and plagioclase; **b)** the diagram 2Ca+3Na/K versus Al/K indicates a lower proportion of plagioclase removal relative to pyroxene (0.40 to 0.60, respectively); **c)** Pearce element 2Na/K versus Al/K showing that fractionation of a bytownitic plagioclase (An_{82-76}) has been effective in primitive melts (the regression line is *y=0.276x+0.5312* with a correlation coefficient r=0.85); in more evolved melts the fractionating plagioclase is a labradorite (An_{67-62}) (in this case the regression line is *y=0.3576x+0.313* with a correlation coefficient r=0.74). Reference curves for fractionation of anorthite (An_{100}) and albite (An_0) are also reported for comparison.

1381

1382 **Fig. 6.** Thermobarometry of melt inclusions in olivine in primitive Stromboli basalts and pumices
1383 erupted at Stromboli. **(a)** *P-T* estimates for the equilibrium crystallization of primitive Stromboli
1384 basalts (preserved in melt inclusions). The graph summarizes the *P-T* grid obtained by solving
1385 thermodynamically reactions (1) and (2) indicated by the large numbers in parentheses. Smaller
1386 numbers are the water contents within the melt (wt% H_2O). Best solutions are outlined by
1387 rectangles (see text and Table A1). **(b)** P-T estimates for ultracalcic melt inclusions following the
1388 same procedure indicated above. Note that these melts equilibrate at moderately higher
1389 temperatures and slightly lower pressures than these reported above (Fig. 6b, Table A2).
1390 **(c)** *P-T* estimates for the crystallisation of the mineral phases of the pumices. In this case best
1391 estimates are obtained by solving thermodynamically reaction (2) and (3). See text and Table A3**.**
1392

1393 **Fig. 7.** Schematic sketch of phase stabilities for Stromboli primitive basalt and suggested *P-T* paths
1394 during decompression. Phase stabilities are consistent with previously discussed equilibria and the
1395 experimental data of Di Carlo *et al.* (2006), Pichavant *et al*., 2009. The stability field of the low
1396 pressure assemblage has been reconstructed following Cigolini *et al*. (2008) and the experimental
1397 work of Conte et al. (2006). Average primitive melt inclusions and ultracalcic melts are represented
1398 by white and grey squares, respectively (with their relative standard deviations, see Tables 5 and 6,
1399 see text). The average of evolved melt inclusions found in Fo_{70} of the scorias are represented by a
1400 white circle (see Table 7 and 8). Line (a) represents the final decompression of the evolved
1401 Stromboli basalt erupted as scoria or lava; line (b) is the possible final *P-T* path associated with the
1402 ejection of pumices during paroxysmal explosions.
1403

1404 **Fig. 8.** Sulphur degassing rate (SO_2 flux - left axis) recorded between 27 February 2007 (the onset
1405 of the effusive activity) and 15 October 2007. This period was characterized by anomalous
1406 degassing rates, that exceeded average values recorded during the typical strombolian activity

(~100 ton/day). The SO_2 flux data are from INGV, available at http://www.pa.ingv.it/comunicati/Stromboli/comunicati_stromboli.php.

On the right axis, sulphur emissions were converted into volumetric flux of magma degassing (Q_{degas}), by using the petrologic method (see text for details). The trend obtained was fitted by using an "exponential + offset" equation (dashed line), where the offset component represents to the magma supply rate during the typical strombolian activity ($Q_{in,steady}$ – cf. bottom of the graph) and the exponential component represents to the "excess" of magma supply rate recorded during and after the 2007 effusive activity ($Q_{in,ex}$ – stippled field). The exponential trend retrieved for $Q_{in,ex}$ is ascribed to decompression from deep storage zone.

Fig. 9. Representative graphs that synthesize the isothermal decompression of a primitive Stromboli basalt (the selected melt is the average of melt inclusions reported in Table 5; see Appendix 5 for calculations). **(a)** Solubility of water and carbon dioxide as a function of pressure (for a temperature of 1170 °C) and **(b)** cumulative gas volume fraction during decompression calculated according to VOLATILECALC (Newman & Lowerstern 2002). **(c)** Variation of compressibility for the above primitive Stromboli basalt during decompression due to bubble growth and crystallization (see text for details).

1431 **Fig. 1**

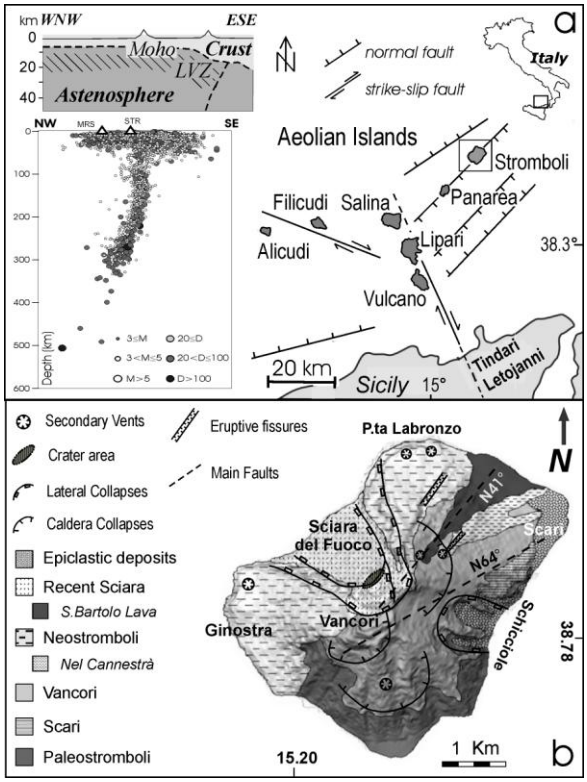

1432

1433 **Fig. 2**

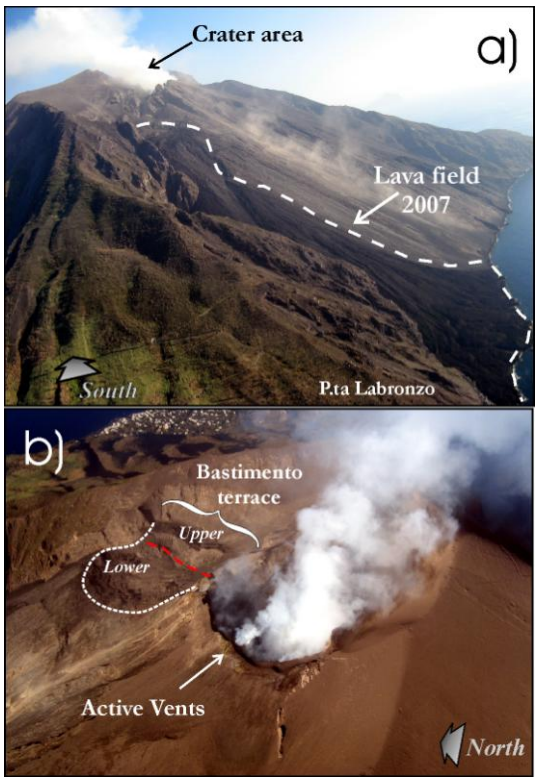

1434

Fig. 3

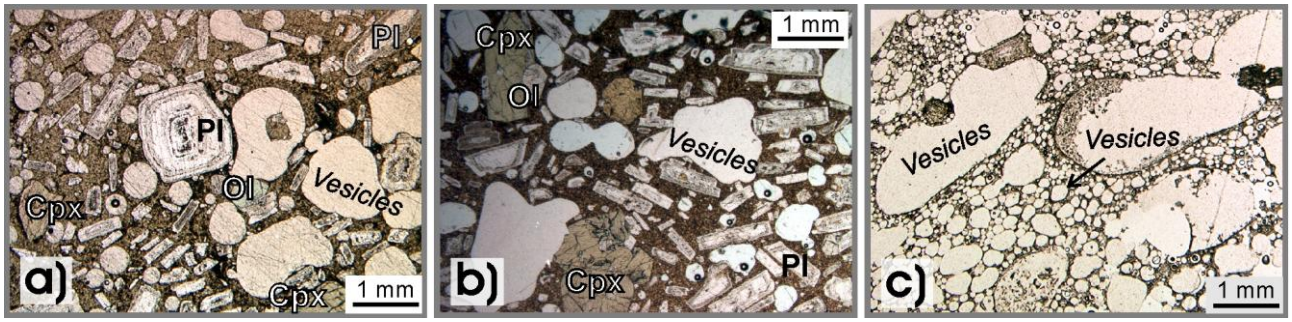
Pl
Pl
Cpx
Ol
Vesicles
a)
Cpx
1 mm
Cpx
Ol
1 mm
Vesicles
b)
Cpx
Pl
Vesicles
Vesicles
c)
1 mm

Fig. 4

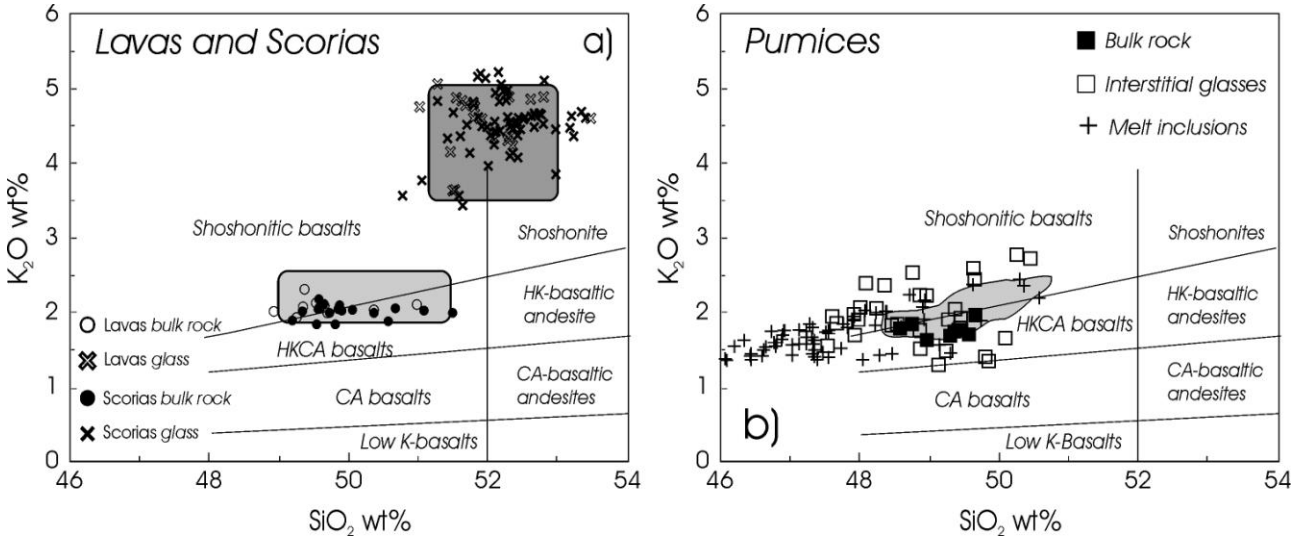
Lavas and Scorias
a)
Shoshonitic basalts
Shoshonite
HK-basaltic andesite
HKCA basalts
CA-basaltic andesites
CA basalts
Low K-basalts
Lavas bulk rock
Lavas glass
Scorias bulk rock
Scorias glass
K2O wt%
SiO2 wt%
Pumices
Bulk rock
Interstitial glasses
Melt inclusions
Shoshonitic basalts
Shoshonites
HK-basaltic andesites
HKCA basalts
CA-basaltic andesites
CA basalts
Low K-Basalts
b)
K2O wt%
SiO2 wt%

Fig. 5

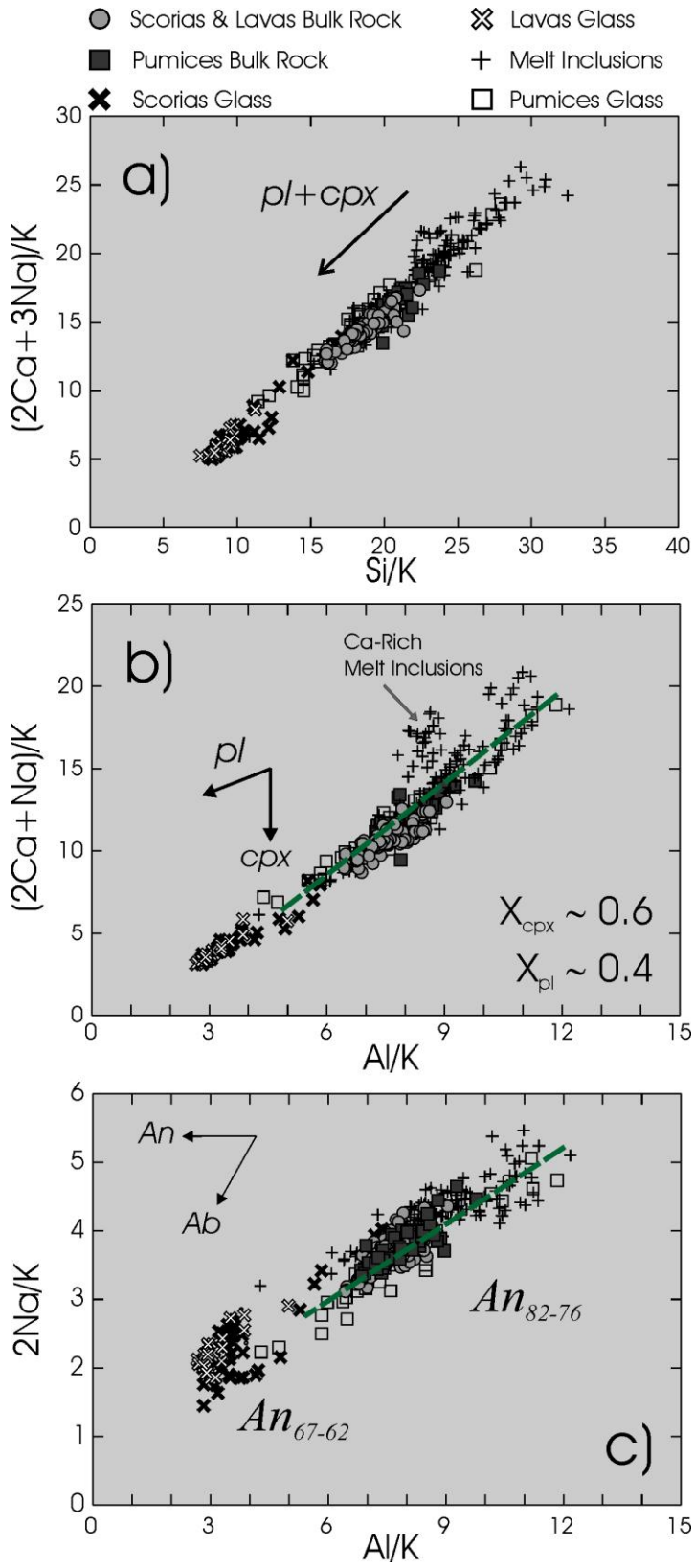
Scorias & Lavas Bulk Rock
Pumices Bulk Rock
Scorias Glass
Lavas Glass
Melt Inclusions
Pumices Glass
a)
pl+cpx
(2Ca+3Na)/K
Si/K
b)
Ca-Rich
Melt Inclusions
pl
cpx
X_cpx ~ 0.6
X_pl ~ 0.4
(2Ca+Na)/K
Al/K
An
Ab
An82-76
An67-62
c)
2Na/K
Al/K

Fig. 6

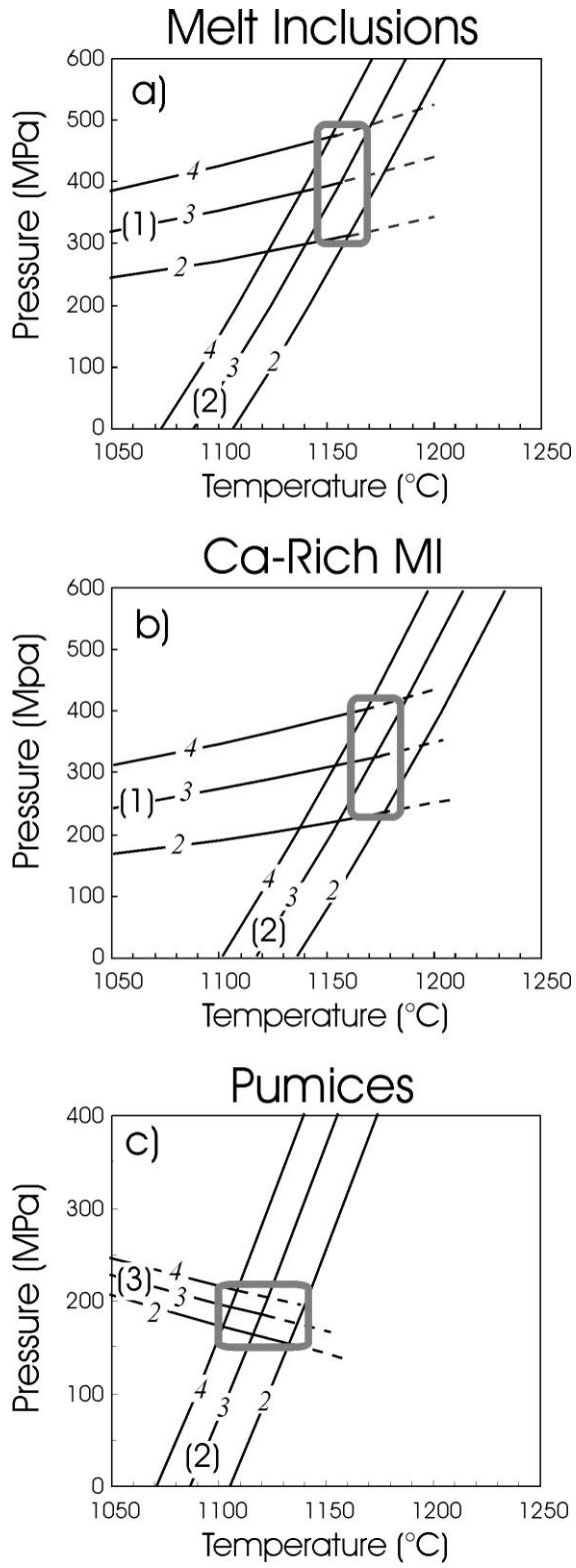
Melt Inclusions
a)
Pressure (MPa)
Temperature (°C)
(1)
(2)
Ca-Rich MI
b)
Pressure (Mpa)
Temperature (°C)
(1)
(2)
Pumices
c)
Pressure (MPa)
Temperature (°C)
(3)
(2)

Fig. 7

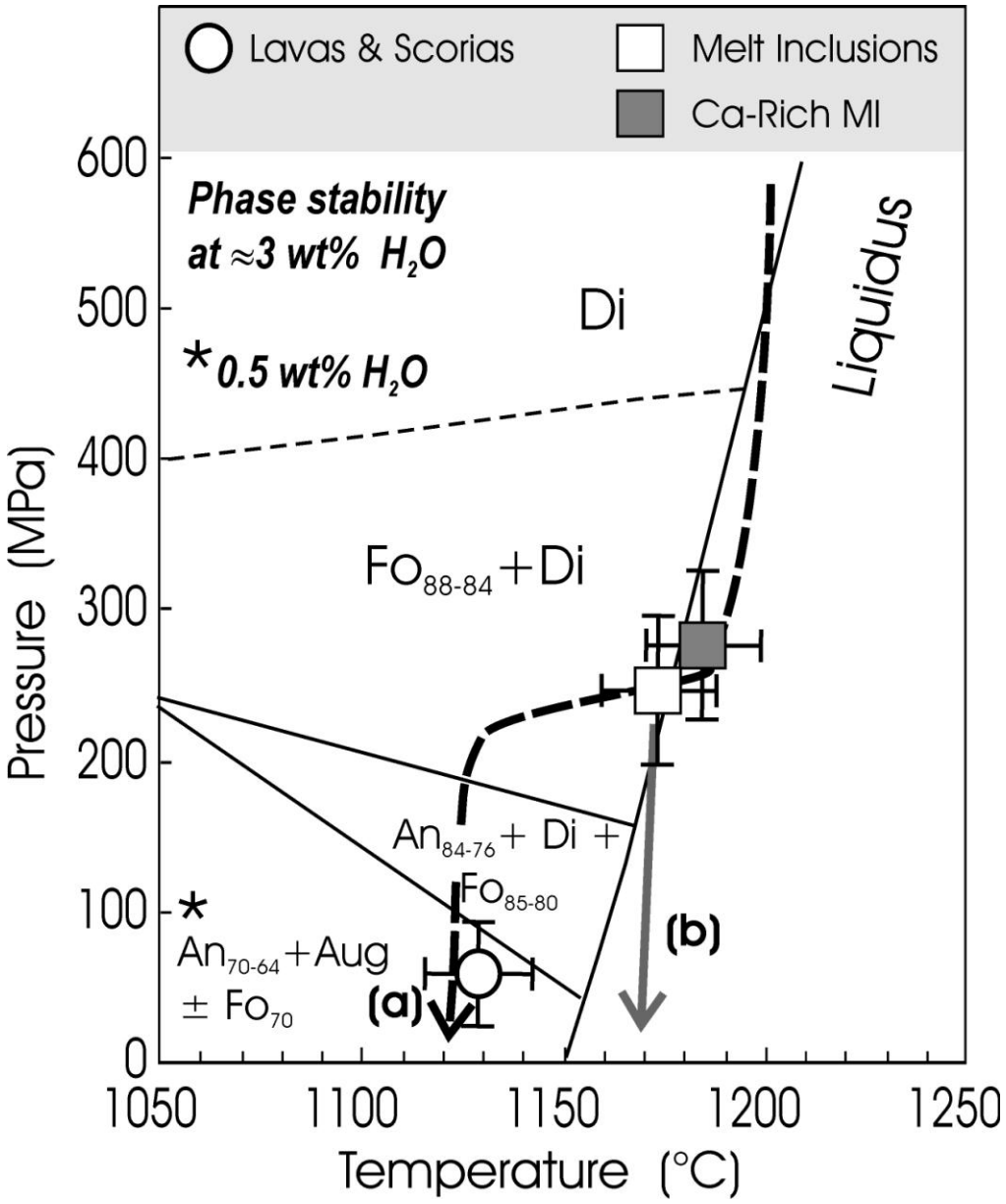
Lavas & Scorias
Melt Inclusions
Ca-Rich MI
Phase stability
at ≈3 wt% H2O
*0.5 wt% H2O
Di
Liquidus
Fo88-84 + Di
An84-76 + Di +
Fo85-80
*
An70-64 + Aug
± Fo70
(a)
(b)
Pressure (MPa)
Temperature (°C)
0
100
200
300
400
500
600
1050
1100
1150
1200
1250

Fig. 8

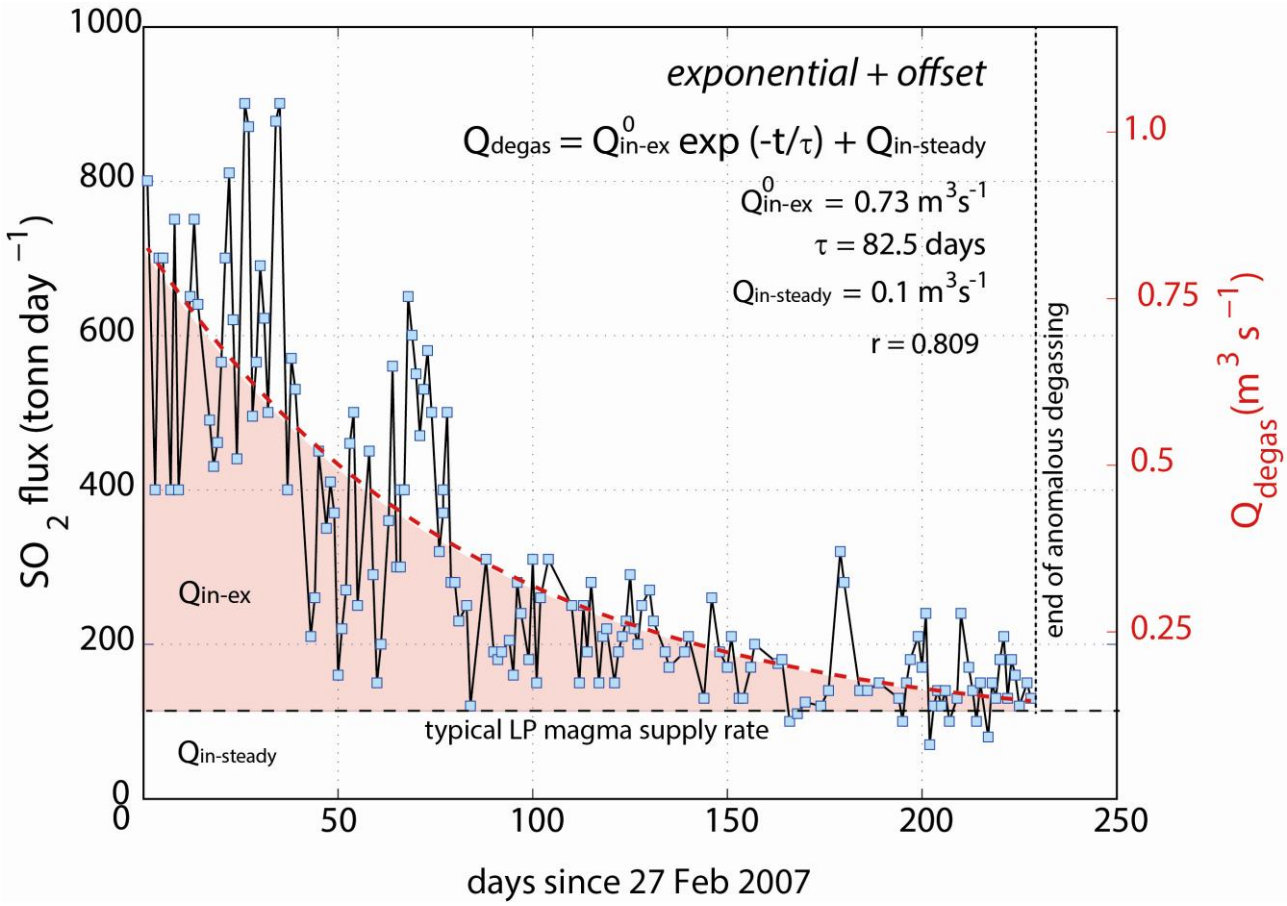
exponential + offset
$Q_{degas} = Q^{0}_{in\text{-}ex} \exp(-t/\tau) + Q_{in\text{-}steady}$
$Q^{0}_{in\text{-}ex} = 0.73\ m^3 s^{-1}$
$\tau = 82.5$ days
$Q_{in\text{-}steady} = 0.1\ m^3 s^{-1}$
r = 0.809
SO_2 flux (tonn day^{-1})
Q_{degas} (m^3 s^{-1})
$Q_{in\text{-}ex}$
$Q_{in\text{-}steady}$
typical LP magma supply rate
end of anomalous degassing
days since 27 Feb 2007
0
200
400
600
800
1000
0.25
0.5
0.75
1.0
50
100
150
200
250

1470 **Fig. 9**

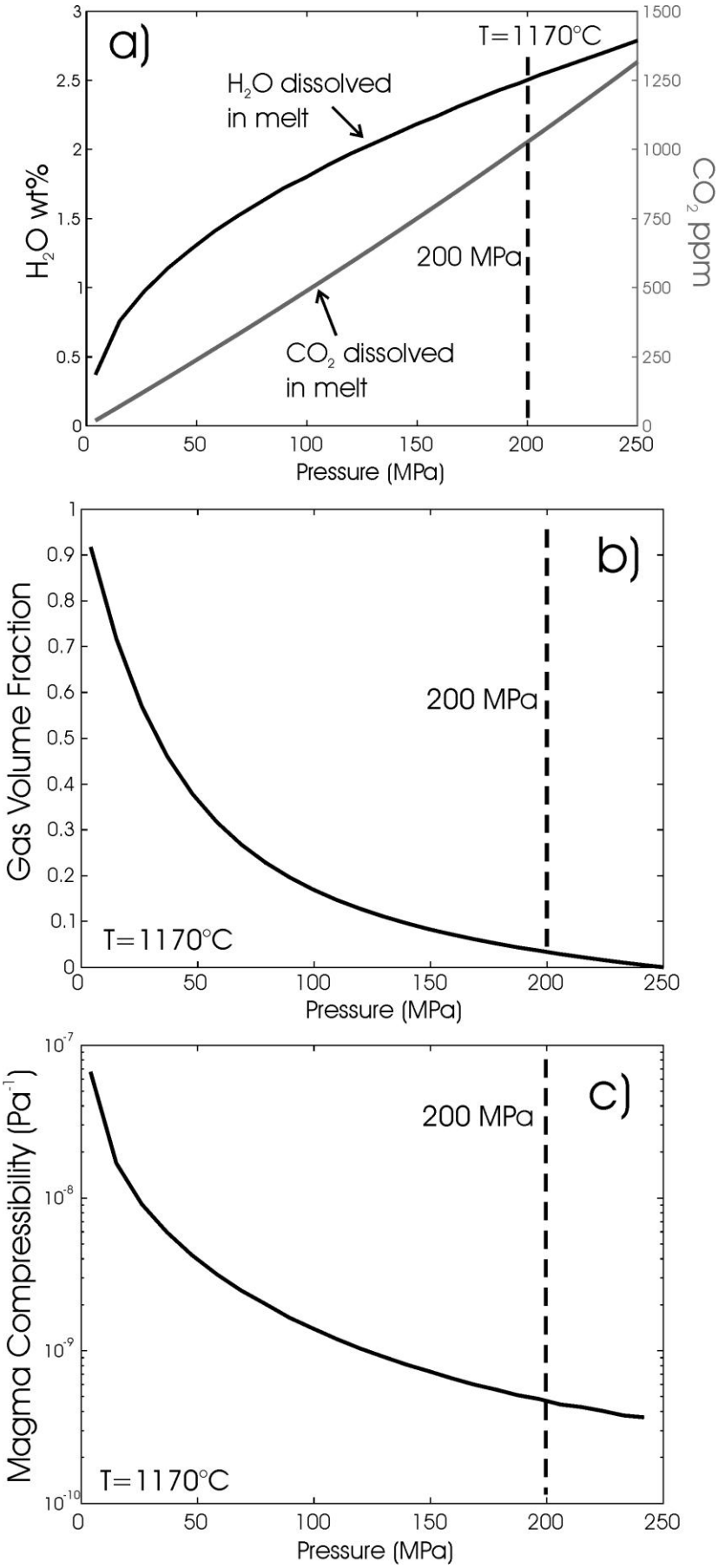

1471

Table A1. *Summary of selected thermodynamic solutions of solid-liquid equilibria for melt inclusions in olivines of the pumices erupted during paroxysmal events. See text and Fig. 6 for details*

Reaction (1)	**Fo (sol) + SiO_2 = CEn**			**Hydrous melt with H_2O = 3 wt %**	
T (°C)	**a_{Fo}**	**a_{CEn}**	$\Delta G_0^{1,T}$ (kJ)	**log a_{SiO2}**	**P (MPa)**
1000	0.7785	0.5563	-6.2297	-0.4894	288
1100	0.7730	0.4857	-5.0144	-0.4918	354
1125	0.7717	0.4710	-4.6908	-0.4923	374
1150	0.7705	0.4572	-4.3595	-0.4928	395
1175	0.7693	0.4442	-4.0207	-0.4933	417
1200	0.7682	0.4320	-3.6743	-0.4938	440
1250	0.7661	0.4098	-2.9592	-0.4947	490
Reference	Sack & Ghiorso (1989)	Gasparik (1990)		Ghiorso & Sack (1995)	

Reaction (2)	**Di = 1/2SiO_2(liq) + 1/2Ol(liq) + Wo(liq)**				**Hydrous melt with H_2O = 3 wt %**	
P (MPa)	**a_{Di}**	**$a_{Wo(liq)}$**	**$a_{Fo(liq)}$**	$\Delta G_0^{1,T}$ (kJ)	**log a_{SiO2}**	**T (°C)**
10	0.8461	0.1082	0.0475	46.8242	-0.4920	1089
100	0.8460	0.1086	0.0476	46.1747	-0.4923	1105
200	0.8458	0.1090	0.0477	45.4615	-0.4927	1122
300	0.8457	0.1094	0.0479	44.7580	-0.4931	1139
400	0.8455	0.1098	0.0480	44.0649	-0.4934	1155
600	0.8453	0.1104	0.0482	42.7123	-0.4940	1186
800	0.8451	0.1111	0.0483	41.4069	-0.4945	1214
Reference	Gasparik (1990)	Ghiorso & Sack (1995)	Ghiorso & Sack (1995)		Ghiorso & Sack (1995)	Ghiorso & Sack (1995)

the melt composition is the average Melt Inclusions in Table 1; olivine and clinopyroxene are analyses n. 1 and n.14 in Table 2. Calculations are referred to an hydrous melt with 3 wt% H_2O.

Table A2. *Summary of selected thermodynamic solutions of solid-liquid equilibria for Ultracalcic melt inclusions in olivines of the pumices erupted during paroxysmal events. See text and Fig. 6 for details*

Reaction (1)	**Fo (sol) + SiO_2 = CEn**			**Hydrous melt with H_2O = 3 wt %**	
T (°C)	**a_{Fo}**	**a_{CEn}**	$\Delta G_0^{1,T}\ (kJ)$	**log a_{SiO2}**	**P (MPa)**
1000	0.8184	0.5336	-6.2297	-0.5087	218
1100	0.8152	0.4654	-5.0144	-0.5119	274
1125	0.8144	0.4512	-4.6908	-0.5127	291
1150	0.8137	0.4378	-4.3595	-0.5134	310
1175	0.8130	0.4253	-4.0207	-0.5141	329
1200	0.8123	0.4136	-3.6743	-0.5147	349
1250	0.8111	0.3922	-2.9592	-0.5160	394
Reference	Sack & Ghiorso (1989)	Gasparik (1990)		Ghiorso & Sack (1995)	

Reaction (2) **Di = 1/2SiO_2(liq) + 1/2Ol(liq) + Wo(liq)**					**Hydrous melt with H_2O = 3 wt %**	
P (MPa)	**a_{Di}**	**$a_{Wo\ (liq)}$**	**$a_{Fo\ (liq)}$**	$\Delta G_0^{1,T}\ (kJ)$	**log a_{SiO2}**	**T (°C)**
10	0.8485	0.1314	0.0502	45.6083	-0.5129	1119
100	0.8484	0.1318	0.0504	44.9349	-0.5134	1135
200	0.8482	0.1323	0.0505	44.1970	-0.5139	1152
300	0.8481	0.1327	0.0507	43.4706	-0.5143	1169
400	0.8480	0.1332	0.0508	42.7564	-0.5148	1185
600	0.8478	0.1339	0.0511	41.3662	-0.5156	1215
800	0.8476	0.1346	0.0513	40.0289	-0.5163	1243
Reference	Gasparik (1990)	Sack & Ghiorso (1989)	Sack & Ghiorso (1989)		Ghiorso & Sack (1995)	

the melt composition is the average Ca-Rich Melt Inclusions in Table 1; olivine and clinopyroxene: analyses n. 4 and n.13 in Table 2. Calculations are referred to an hydrous melt with 3 wt% H_2O.

Table A3. *Summary of selected thermodynamic solutions of solid-liquid equilibria for bulk rock pumices erupted during paroxysmal events. See text and Fig. 6 for details*

Reaction (2) **Di = 1/2SiO$_2$(liq) + 1/2Ol(liq) + Wo(liq)**					**Hydrous melt with H$_2$O = 3 wt %**	
P (MPa)	**a_{Di}**	**$a_{Wo(liq)}$**	**$a_{Fo(liq)}$**	$\Delta G_0^{1,T}$ (kJ)	**log a_{SiO2}**	**T (°C)**
10	0.8485	0.1084	0.0477	46.8573	-0.4967	1090
100	0.8484	0.1088	0.0479	46.2083	-0.4970	1106
200	0.8482	0.1092	0.0480	45.4956	-0.4972	1124
300	0.8481	0.1096	0.0481	44.7926	-0.4975	1141
400	0.8480	0.1099	0.0483	44.1000	-0.4977	1157
600	0.8478	0.1106	0.0485	42.7481	-0.4981	1187
800	0.8476	0.1112	0.8112	41.4434	-0.4985	1215
Reference	Gasparik (1990)	Ghiorso & Sack (1995)	Ghiorso & Sack (1995)		Ghiorso & Sack (1995)	

Reaction (3)	**An+2Fo+SiO$_2$=2CEn+CaTs**				**Hydrous melt with H$_2$O = 3 wt %**		
T (°C)	**a_{An}**	**a_{Fo}**	**a_{CEn}**	**a_{CaTs}**	$\Delta G_0^{1,T}$ (kJ)	**log a_{SiO2}**	**P (MPa)**
1000	0.7539	0.7785	0.5563	0.0465	31.0489	-0.4937	256
1100	0.7456	0.7730	0.4857	0.0458	34.3173	-0.4956	194
1125	0.7438	0.7717	0.4710	0.0457	35.1677	-0.4960	179
1150	0.7420	0.7705	0.4572	0.0455	36.0314	-0.4964	165
1175	0.7402	0.7693	0.4442	0.0454	36.9086	-0.4968	152
1200	0.7386	0.7682	0.4320	0.0453	37.7992	-0.4971	139
1250	0.7354	0.7661	0.4098	0.0450	39.6207	-0.4978	116
Reference	Newton et al. (1980)	Sack & Ghiorso (1989)	Gasparik (1990)	Gasparik (1984)		Ghiorso & Sack (1995)	

the melt composition is the average Recent Pumices reported in Table 1; olivine and clinopyroxene: analyses n. 1 and n.14 in Table 2; plagioclase: analysis n. 20 in Table 2. Calculations refer to an hydrous melt (3 wt% H_2O)

Table A4. *List of symbols for the physical parameters used in thermodynamic calculations and geophysical modeling. See text for details.*

Symbol	Unit	Description
Thermodynamics		
$\Delta G_0^{P,T}$	$kJ\ mol^{-1}$	Gibbs free energy at the P and T of interest
$\Delta G_0^{1,T}$	$kJ\ mol^{-1}$	Gibbs free energy at *1 bar* and T of interest
R	$J\ mol^{-1}\ K^{-1}$	Gas constant
K_i	*adim.*	Equilibrium constant for a generic reaction *i*
ΔV	$J\ bar^{-1}$	Difference of the molar volumes of the products minus those of the reactants opportunely expanded and compressed at P and T of interest
a_i	*adim.*	activity of a generic phase i (calculated according to solution models, see text)
f_{O_2}	*bar*	oxygen fugacity
$X_{H_2O}^m$	*adim.*	mole fraction of water in the melt
$X_{CO_2}^m$	*adim.*	mole fraction of CO_2 in the melt
Geophysical Parameters		
Q_{degas}	$m^3\ s^{-1}$	total magma degassing rate
M_S	$g\ mol^{-1}$	sulphur molecular mass
M_{SO_2}	$g\ mol^{-1}$	sulphur dioxide molecular mass
$\phi\ SO_2^*$	$kg\ s^{-1}$	sulphur degassing rate
ρ_M	$kg\ m^{-3}$	density of the magma
$Q_{in\text{-}steady}$	$m^3\ s^{-1}$	magma input rate during steady state
$Q_{in\text{-}ex}$	$m^3\ s^{-1}$	magma input rate in excess
$V_{in\text{-}steady}$	$m^3\ x10^6$	magma volume entering in the degassing zone during steady state
$V_{in\text{-}ex}$	$m^3\ x10^6$	magma volume in excess entering in the degassing zone
V_{out}	$m^3\ x10^6$	generic volume transferred outside the chamber
V_R	$m^3\ x10^6$	total volume of the reservoir
t	*days*	time since the begininng of eruption
τ	*days*	time constant of the exponential decay
C	$m^3\ Pa^{-1}$	capacity of the reservoir
R_e	$Pa\ s\ m^{-3}\ x10^6$	resistance of the conduit
ρ_e	$kg\ m^{-3}$	density of the erupted magma
P_0	$Pa\ x10^6$	initial overpressure
β_R	Pa^{-1}	wallrock compressibility
β_M	Pa^{-1}	magma compressibility
ρ_l	$kg\ m^{-3}$	density of the liquidus
ρ_g	$kg\ m^{-3}$	density of the gas mixture

* SO_2 values are from the Istituto Nazionale di Geofisica e Vulcanologia, INGV http://www.pa.ingv.it/comunicati/Stromboli/comunicati_stromboli.php

Table A5. *Summary of the main physical parameters calculated for the isothermal decompression path of the Stromboli primitive melt*

Reference Melt		**Starting Conditions**	
	wt%		
SiO_2	47.6	**T (°C)**	1170
TiO_2	0.86	**P (MPa)**	250
Al_2O_3	15.3	**H_{melt} (kg/m^3)**	2694
FeO_T	7.67	**$H_{crystal}$ (kg/m^3)**	3270
MnO	0.14	**H_R^{-1} (Pa^{-1})**	3^{-11}
MgO	6.37	**Crystals Fraction**	0
CaO	12.9		
Na_2O	2.20		
K_2O	1.58		
P_2O_5	0.49		
S	0.16		
Cl	0.15		
H_2O	2.79		
CO_2 (ppm)	1320		

Results

P*	H_2O*	CO_2*	H_2O exs*	CO_2 exs*	$H_{gas\ mixture}$**	H_{liquid} †	Gas Volume Fraction	H_{melt} ‡	Crystals Fraction	H_M ‡
MPa	wt%	ppm	wt%	ppm	kg/m^3	kg/m^3		kg/m^3		Pa^{-1}
233	2.69	1215	0.097	104	469	2691	0.010	2677	0	**3.77^{-10}**
215	2.59	1111	0.199	208	444	2688	0.022	2659	0	**4.27^{-10}**
206	2.54	1059	0.252	260	431	2687	0.029	2696	0.1	**4.45^{-10}**
197	2.48	1007	0.308	312	417	2686	0.036	2684	0.1	**4.83^{-10}**
178	2.37	903	0.423	416	388	2683	0.052	2658	0.1	**5.57^{-10}**
159	2.24	799	0.546	520	357	2680	0.072	2634	0.2	**6.61^{-10}**
140	2.11	695	0.679	624	322	2677	0.096	2592	0.2	**8.12^{-10}**
120	1.97	591	0.824	728	285	2675	0.128	2565	0.3	**1.04^{-9}**
109	1.89	539	0.903	780	265	2673	0.147	2530	0.3	**1.19^{-9}**
100	1.80	487	0.986	832	245	2672	0.170	2489	0.3	**1.40^{-9}**
79	1.62	383	1.169	936	201	2669	0.229	2377	0.3	**2.03^{-9}**
58	1.41	279	1.383	1040	152	2665	0.317	2219	0.4	**3.17^{-9}**
37	1.14	175	1.653	1144	100	2662	0.461	1888	0.4	**5.98^{-9}**
15	0.76	71	2.034	1248	42	2659	0.716	1159	0.4	**1.69^{-8}**

* - VOLATILECALC (Newman & Lowenstern, 2002); ** - Holloway (1977); † - Lange & Carmichael (1990); ‡ - Huppert & Woods (2002)
exs: exsolved gas concentration